Extraction of Zinc and Iron from Steel Dust Waste

Tien Chan Wai

A project report submitted in partial fulfilment of the requirements for the award of Bachelor of Engineering (Honours) Mechanical Engineering

Lee Kong Chian Faculty of Engineering and Science
Universiti Tunku Abdul Rahman

May 2020

DECLARATION

I hereby declare that this project report is based on my original work except for citations and quotations which have been duly acknowledged. I also declare that it has not been previously and concurrently submitted for any other degree or award at UTAR or other institutions.

Signature : 

Name : Tien Chan Wai

ID No. : 1503323

Date : 18-05-2020

APPROVAL FOR SUBMISSION

I certify that this project report entitled **"Extraction of Zinc and Iron from Steel Dust Waste"** was prepared by **Tien Chan Wai** has met the required standard for submission in partial fulfilment of the requirements for the award of Bachelor of Engineering (Honours) Mechanical Engineering at Universiti Tunku Abdul Rahman.

Approved by,

Signature	:	
Supervisor	:	Dr. Lee Hwang Sheng
Date	:	18-05-2020

Signature	:	NIL
Co-Supervisor	:	NIL
Date	:	NIL

ACKNOWLEDGEMENTS

The completion of this research project would never have been possible without the assistance and support of many individuals. First and foremost, I would like to express my deepest gratitude to my supervisor, Dr. Lee Hwang Sheng for his great advice, invaluable assistance, constructive comment and enormous patience throughout the project. Moreover, the technical contribution of UTAR is truly appreciable.

In addition, I would also like to express my gratitude to my loving parents who gave me tremendous encouragement. It has been a great pleasure working together with Dr. Lee Hwang Sheng's Final Year Project students, Ms. Yee Shiuan Yiing, Mr Ang Xi Ze and Mr Chua Kee Yean.

ABSTRACT

Electric Arc Furnace Dust (EAFD) is a toxic by-product released from EAF steelmaking process. Conventional solution of landfilling EAFD is destroying environment and public health due to the presence of heavy metals such as zinc, iron, nickel and lead. Hence, it is necessary to develop cost effective and feasible remediation solutions to cope with increasing demand of treating EAFD waste. Zinc (Zn) and iron (Fe) which contribute to the largest composition of EAFD (approximately 10-50 wt% and 16-60wt% respectively) can be recycled through extraction and precipitation as easy filterable precipitates. This project focused on maximum extraction amount of zinc and iron through EAFD leaching in hydrochloric acid (HCl) using hydrometallurgical method followed by precipitation of leaching solution using sodium hydroxide (NaOH) to form iron oxide and zinc oxide eventually. For leaching, the acid concentration, temperature, experiment duration, dust-to-acid ratio, and stirring speed were fixed at 10M, 50 ℃, 15 minutes, 1:30, and 700 rpm, respectively. The results (almost 100% zinc and iron extraction) were obtained. After leaching, only traces of carbon exist in the residues, while zinc and iron were completely dissolved. For precipitation, the alkali concentration and stirring speed were fixed at 0.5M and 400 rpm at room temperature condition. NaCl and $Fe(OH)_3$ were obtained when the pH of the solution was increased to 5 by NaOH solution. Subsequently, $Zn_5(OH)_8Cl_2 \cdot H_2O$ and NaCl were achieved when the pH of the solution was increased to 6.34. TGA results suggested hematite was formed when pH 5 precipitate was heated at 240 ℃ in nitrogen atmosphere. Besides, TGA results also suggested zinc oxide was formed when pH 6.34 precipitate was heated up to 180 ℃ in nitrogen atmosphere. The results in this project indicated the feasibility of zinc and iron extraction from EAFD through leaching and precipitation which will be beneficial to solve the dust waste problems in steel industries.

TABLE OF CONTENTS

LIST OF TABLES

LIST OF FIGURES

LIST OF SYMBOLS / ABBREVIATIONS

ρ	Density, g/ml
M	Molarity, M
P	Pressure, kPa
T	Temperature, ℃
BOF	Blast oxygen furnace
Cd	Cadmium
Cr	Chromium
EAF	Electric arc furnace
EAFD	Electric Arc Furnace dust
Fe	Iron
$FeCl_2$	Iron (II) chloride
$FeCl_3$	Iron (III) chloride
Fe_2O_4	Hematite
Fe_3O_4	Magnetite
$Fe(OH)_3$	Iron (III) hydroxide
H_2SO_4	Sulphuric acid
HCl	Hydrochloric acid
Mg	Manganese
Mn	Magnesium
NaCl	Sodium chloride
NaOH	Sodium hydroxide
$NaHCO_3$	Sodium bicarbonate
NH_4OH	Ammonium hydroxide
Ni	Nickel
ppm	Parts per million
S	Sulphur
Si	Silicone
Zn	Zinc
$ZnCl_2$	Zinc chloride
$ZnFe_2O_4$	Zinc ferrite
$Zn_5(OH)_8Cl_2 \cdot H_2O$	Zinc chloride hydroxide monohydrate

ZnO	Zinc Oxide

LIST OF APPENDICES

CHAPTER 1

INTRODUCTION

1.1 General Introduction

Steelmaking industry being one of the main arteries of the industry since the second industrial revolution, continues to be in demand and will be expanding in the coming decade due to the increasing usage of steel in diverse industries. In local front, the steelmaking industry centred on two primary types of products - long steel products (steel bars, wire rods, rebars and beams) which are used in construction; and flat steel products (coated sheets, plates, hot rolled sheets and cold rolled sheets) which are used in machinery, automotive and oil gas industries (Liew, 2019). Basically, steelmaking industry today can be divided into BOF steelmaking process and EAF steelmaking process. BOF steelmaking process uses 95% iron ore, 5% steel scrap as raw material, while EAF steelmaking process uses 100% steel scrap as raw material. Major advantages such as complete recycling of steel, large reduction in specific energy and flexibility in varying production according to demand causing EAF steelmaking process better competitive edge than BOF steelmaking process.

At the stage of melting with extreme condition, volatile elements, for examples, Zn, Pb and Cd volatilized and contributed to the formation of flue dust known as EAFD. Generally, 10 to 20 kg of EAFD are collected per tonne of steel from EAF steelmaking process. In most industrialized and developed countries in the world, EAFD with heavy metals composition is officially listed and treated as hazardous waste. Conventionally, EAFD has been dumped and landfilled directly at a great financial cost. Nevertheless, the depletion of site available for landfill, social pressures and environmental concern encourage steel manufacturing companies to take advantage of sustainable recycling options that allow the recovery of valuable minerals such as Zn and Fe without damaging their metallurgical characteristics. In general, the presence of Zn mostly can be found in two basic compounds, namely as franklinite ($ZnFe_2O_4$) and zincite (ZnO), whereas Fe exists in oxide forms such as hematite (Fe_2O_3) and magnetite (Fe_3O_4). EAFD usually contains 10-50 wt% of Zn and 16-60wt% of Fe.

Current technologies for EAFD treatment are predominantly pyrometallurgical methods where typically the EAFD is recycled via Waelz Kiln process. Downsides of this high temperature reduction process are high consumption of electrical cost and

high initial investment, therefore it is only deemed suitable for large volume of EAFD treatment. Although in the past hydrometallurgical methods may not as popular as pyrometallurgical methods, recently hydrometallurgical methods have emerged as an interesting alternative as they can fit on small scale, offer environmental benefits, operate in lower cost and provide higher flexibility. Hydrometallurgical methods of treating EAFD involve acids leaching lixiviant (H_2SO_4, HCl) and alkalis leaching lixiviant (NaOH, NH_4OH) to extract Zn and other existed elements in EAFD. The benefits of using HCl as leaching lixiviant includes effective dissolution of Zn and Fe, capability to break down the structure of $ZnFe_2O_4$, avoiding the formation of harmful mineral called jarosite and removal of toxic elements in chlorides. Furthermore, filtration technique applied using solid-liquid separation is easier in HCl leaching in contrast to H_2SO_4 leaching. The significant factor that affects the extraction process is concentration, which will be studied for the extraction of Zn and Fe from EAFD.

Precipitation of metal salts from alkaline solution is commonly used since acidic heavy metals are neutralized and precipitated as metal hydroxides. NaOH, $NaHCO_3$ and NH_4OH are often used as precipitating agent. Particularly NaOH is chosen to react with leaching solution due to its benefits of relative simplicity, abundant availability and low cost of precipitant. The pH of the leaching solution is commonly at pH 0-2, by increasing pH value, Zn and Fe hydroxides can be precipitated at certain pH values. The precipitated Zn and Fe hydroxides are heated at high temperature to form Zn and Fe oxides.

1.2 Importance of the Study

The results of this project may provide guidelines for optimum conditions to extract maximum Zn and Fe from EAFD and at the same time avoiding unnecessary waste produced during the process. The hydrometallurgical method using HCl as leaching lixiviant and chemical precipitation using NaOH as precipitating agent which will be proposed in this project are comparatively clean and easy to be set up. Hence the successful demonstration of this laboratory scale project will proceed into pilot scale and eventually can be adapted and commercialized in small and medium scale industries. This project is beneficial to solve the dust waste problems in steel industries.

1.3 Problem Statement

In Malaysia, conventional landfill is used to dispose EAFD. However, considering the steel manufacturing industry is continuing to expand with a growing economy, a massive increase in operational cost is required in the perspective of getting land and licence for landfill. Deforestation to create more landfill sites is one of the concerns. When rain falls on landfill sites, the heavy metals will be leached out and this can result in severe contamination of groundwater.

The limitations of pyrometallurgical method are capability of processing EAFD economically only in high volume production, high energy consumption and production of impure ZnO which has low commercial value. These impure ZnO require subsequent hydrometallurgical method to be refined and recycled, thus this is not inducive to the sustainability. Hydrometallurgical method could offer an interesting alternative in treating EAFD, unfortunately most of the literatures merely concentrates on the leaching of Zn and controlled dissolution of Fe because the structure of $ZnFe_2O_4$ was reported difficult to be broken, thus favouring the recovery of Zn only. The possibility to leach out Fe in the EAFD has been heavily overlooked. Regardless of the type of leaching lixiviant used, the leaching process usually produces Zn and Fe compound in the form of aqueous solution. The question remains whether Zn and Fe compound in solid form can be produced in order to provide more flexibility and workability for engineering and manufacturing industry. This project represents the overview of the designing of experiment to extract Zn and Fe from EAFD under with the aim of zero waste generation.

1.4 Aim and Objectives

The aim of this project is to investigate the extraction of zinc and iron from EAFD. The objectives of this project are:

I. To determine the extraction amount of Zn and Fe from EAFD using 10M of HCl.
II. To investigate the precipitation of different types of metal oxides from leaching solution at different pH values.
III. To characterize the composition and morphology of EAFD.

1.5 Scope and Limitation of the Study

This research focuses on maximum extraction of Zn and Fe with hydrometallurgical method using HCl at following constant conditions: 10M HCl, 50 °C leaching temperature, 15 minutes leaching duration, 700 rpm stirring speed and dust-to-acid ratio of 1:30. The amount of Zn and Fe in raw EAFD are identified using Inductively Coupled Plasma Optical Emission Spectroscopy (ICP-OES). During the leaching process, condenser and conical flask are used to recycle evaporated HCl fume back to the HCl solution to reduce waste contamination. The leaching solution and NaOH are used as precursors to precipitate metal oxides at different pH values at room temperature. After precipitation, drying and heating are required to remove the impurities on the surface of the precipitate. Upon completion of leaching and precipitation, a series of characterization on leached EAFD and precipitate are performed using the analysis techniques such as SEM-EDX, ICP-OES, TGA and XRD.

1.6 Contribution of Study

This project is an overview of solving the environmental pollution issues caused by improper managing and handling of electric arc furnace dust waste via hydrometallurgy and precipitation. Prior to this study, limited research studies have been done to precipitate metal oxide from leaching solution after hydrometallurgy process. Therefore, in this project, valuable metals such as zinc and iron can be recovered and precipitated in oxides using this approach. Besides, the morphology, mineralogical composition, chemical composition and thermal decomposition of samples were investigated in this project.

1.7 Outline of the Report

In this research project report, it consists of total five main chapters and several sub-chapters under each chapter.

Chapter 1 includes the general introduction and background of EAFD, hydrometallurgy and precipitation, importance of study, problem statement, aim and objectives, scope and limitation of study, contribution of study, ended with outline of the report.

Chapter 2 covers the literature reviews performed by many professionals and researchers.

Chapter 3 explains the overall methodology and work plan of the research which includes sample preparation, experiment setup and advanced instruments used.

Chapter 4 is the core part of this research project which describes, analyses and discusses the results obtained.

Chapter 5 concludes the research project with objectives accomplishment. Several recommendations were proposed for future research improvement.

CHAPTER 2

LITERATURE REVIEW

2.1 Steel Making Process

Steel is the world most well-known construction and engineering material due to its special combination of workability, durability and cost. Bell (2019) has stated that some of the world largest steel manufacturing countries such as Japan, US, China and India, they are accounted for roughly 50% of the world production. Even though methods for steel manufacturing have improved remarkably since industrial production started in the late 19th century, original Bessemer Process which utilizes oxygen to decrease the carbon content in iron remain as the foundation for the modern methods. Today, steel is manufactured via two processes which are BOF steelmaking and EAF steelmaking.

2.1.1 Basic Oxygen Furnace Steelmaking

BOF steelmaking is a type of primary steelmaking which means there is an actual process of taking raw material and making them into steel. Majority of the BOF process is performed in a steel mill because lengthy time of transport from one plant to another cannot be afforded in the fast-paced steelmaking process. BOF is accounted for approximately 70% of world steel production (EUMERCI, 2020). BOF can be divided into three steps which are raw material preparation, blast furnace and basic oxygen furnace.

Raw materials such as iron ore, coke and limestone are prepared before the steelmaking process can begin. Kennison (2014) has stated that iron ore is mined in large scale, grounded to powder form, separated with strong magnets and heated to form marble-size pellets in the end. Coke is formed by heating crushed coals in an airtight oven up to 1150 ℃ to 1350 ℃ up to 12 to 16 hours to induce pyrolysis and removed as solid carbon fuel. Limestone which can remove impurities such as sulphur during the next stage (Blast Furnace) is mined and then crushed to become blast furnace flux.

Blast Furnace refers to a continuous furnace where the raw materials and oxygen rich flues gases are fed. Inside the Blast Furnace can reach up to 1700 ℃ , and the combustion of coke results in more intensified heat (Tauriainen,2015). The iron

ore keeps reducing as the molten iron and slag (oxides and sulphur) are formed and collected at the bottom of the furnace. The molten iron is transported to basic oxygen furnace while the slag is commonly sold to cement manufacturing companies. Aula, et, al. (2012) stated that the use of slag is explored in civil engineering due to its technical properties for instance resistance to abrasion and polishing, bulk density, water absorption and strength.

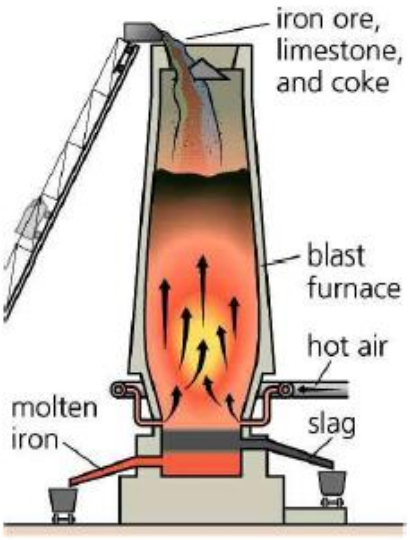

Figure 2.1: Blast Furnace (Kennison, 2014)

Basic oxygen furnace is a furnace that uses oxygen blowing to convert molten iron and ferrous scrap into steel. The oxygen used in the blowing process must has at least 99.5% high purity, or else harmful nitrogen might be absorbed by steel (York, et al., 1999). The term “basic” in the BOF means alkaline material as refractory linings for furnace while the term “oxygen” means oxygen is channeled at supersonic velocity with the aid of a water-cooled lance. The basic oxygen furnace is a refractory-lined, tilted mechanism supported, barrel-shaped steel shell. Besides capability to be held in any position, the vessel can even swing through a vertical plane of 360 degree (York, et al.,1999). Inside basic oxygen furnace, the carbon content of molten iron is reduced from 4-5% to below 1%, and unwanted impurities are removed as slag by limestone (EUMERCI, 2020). If there is no gas recovery system, carbon monoxide is converted to carbon dioxide at the mouth of the furnace. In the end, basic oxygen furnace tilts and pours out the molten steel and send the molten steel for metallurgy process which includes casting or rolling (EUMERCI, 2020).

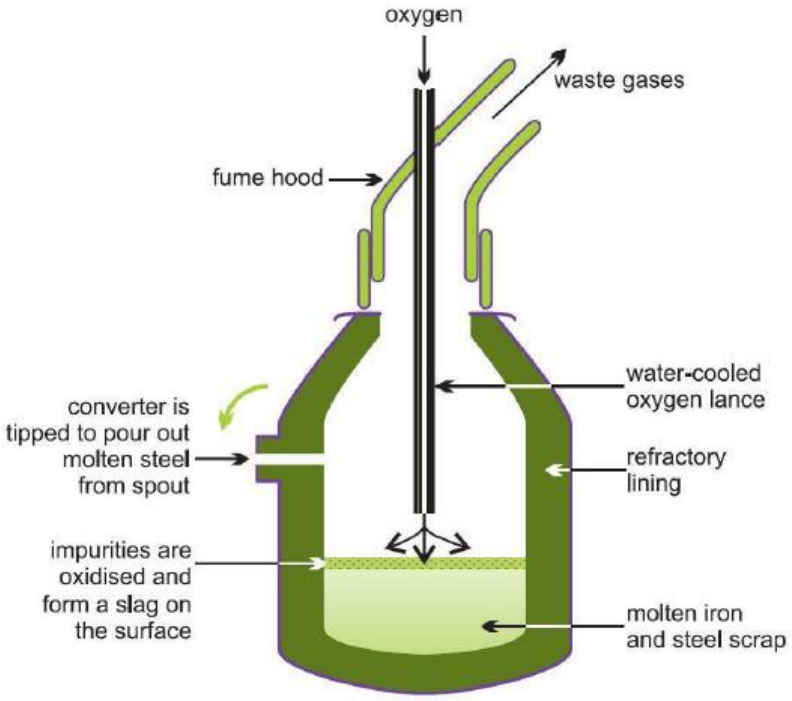

Figure 2.2: Basic oxygen Furnace (EUMERCI, 2020)

2.1.2 Electric Arc Furnace Steelmaking

EAF steelmaking is a secondary steelmaking process which means the crude steel is refined before converting the liquid steel into solid steel. First EAF was designed by Paul Heroult at and the technology has been existing for 100 years (Martín, 2015). EAF steelmaking now accounted for 30% overall of the steelmaking globally and is expected to keep increasing for some time (Martín, 2015). EAF steelmaking is no longer restricted to special steels during 20th century, it has taken off in advancement to replace other steelmaking in the production of high-quality flat products and long products (Martín, 2015). The main purpose of the EAF steelmaking is to convert the raw materials to liquid crude steel as quick as possible and then refine the steel in secondary steelmaking process. EAF steelmaking can be divided into scrap preparation and electric arc furnace.

The prepared scrap used must have a requirement of minimum non-metallic inclusions, particularly for non-ferrous metals and non-magnetic material. Higher content of nitrogen, carbon and residuals will make EAF steelmaking process less attractive for producing ductile, low carbon steels. In order to exclude hazardous contaminants and reduce energy requirement for melting inside furnace, sorting of

scrap and preheating of scrap are performed (EUMERCI, 2020). Afterwards, the scrap is loaded into baskets with magnets or grabs, and prepared for the furnace.

Electric arc furnace can be either alternating current (AC) or direct current (DC). York, et al. (1999) stated that in AC which has 3 electrodes with different phases. The current flows from electrode tip to the bath and then to the next electrode. DC has single or twin electrode, in which the current flows from the electrode via the bath to a return electrode. The electrodes are made of graphite and may be lined with basic or acid refractories. Since the electrodes wear in the process and need to be replaced constantly, the electrodes are designed to be round in section and in segments with treaded couplings , so the new section can be added to the top while slipping the electrode down in the holder arm (York, et al., 1999). Apart from that, the electrodes have special properties of strength and conductivity at high temperature.

The construction of EAF can be split into three sections. Firstly, the shell which is made up of lower steel bowl and walls. The walls are built with water-cooled panels, covered by refractories to reduce the heat loss. Secondly, the hearths which is made up of refractory-lined lower bowl. Shell and heart function to hold the scrap charge during melting and retain the liquid steel until it is ready to be tapped (Aula, et al., 2012). Thirdly, the roof is water-cooled or refractory-lined. Other than consisting of holes for the entering of one or more graphite electrodes, the roof can be swung aside for scrap charging (Aula, et al., 2012).

The process in the EAF began by charging the furnace with scrap from the baskets using overhead crane. Carbon and fluxes (lime and dolomite) are also charged together with the scrap to induce slag formation and prevent overoxidation of steel (EUMERCI, 2020). After charging, the roof is closed, the electrodes are lowered and the meltdown commences. York et al. (1999) has argued that at first low power was set to protect the walls and roof from arc's excessive heat, once the arcs are shielded by scrap sufficiently, power is raised and oxygen is supersonically blown to the scrap. The oxygen is chosen to air because of its support towards decarburization of the melt, exothermic reaction with partially-burnt gases (CO) and hydrocarbon as well as removal of phosphorus and silicon. Martín (2015) stated the oxygen reaction in an EAF as below:

1. Oxidation from solid carbon charged to the furnace (Equation 2.1) and oxidation from carbon from molten steel (Equation 2.2).

$$C\ (s) + \frac{1}{2} O_2\ (g) = CO\ (s) \quad (2.1)$$

$$C + \frac{1}{2} O_2\ (g) = CO\ (s) \quad (2.2)$$

2. Oxidation of Fe to FeO.

$$Fe + \frac{1}{2} O_2\ (g) = FeO \quad (2.3)$$

3. Combustion of hydrocarbons.

$$CH_4\ (g) + \frac{3}{2} O_2\ (g) = CO\ (g) + 2H_2O\ (g) \quad (2.4)$$

4. Post combustion of CO.

$$CO\ (g) + \frac{1}{2} O2\ (g) = CO2\ (g) \quad (2.5)$$

During the meltdown, notably slag (mixture of oxide), which consist mainly of iron, calcium and silicon oxides is formed on the surface of the molten steel. Slag functions to improve energy efficiency during heating through preventing damage to the roof and sidewalls from radiant heat. Following reaching of flat bath condition and complete melt down of scrap, another basket is allowed to be charged into furnace. Finally, when suitable steel temperature and chemistry have been achieved, by tilting the furnace, the steel is tapped out into a preheated ladle and the solidified slag is cleaned at the slag door (York et al., 1999). The steel is then transferred for secondary treatment. On the other hand, the slag is either returned back in melting using magnet or used in road construction mainly in asphalt layer of the road.

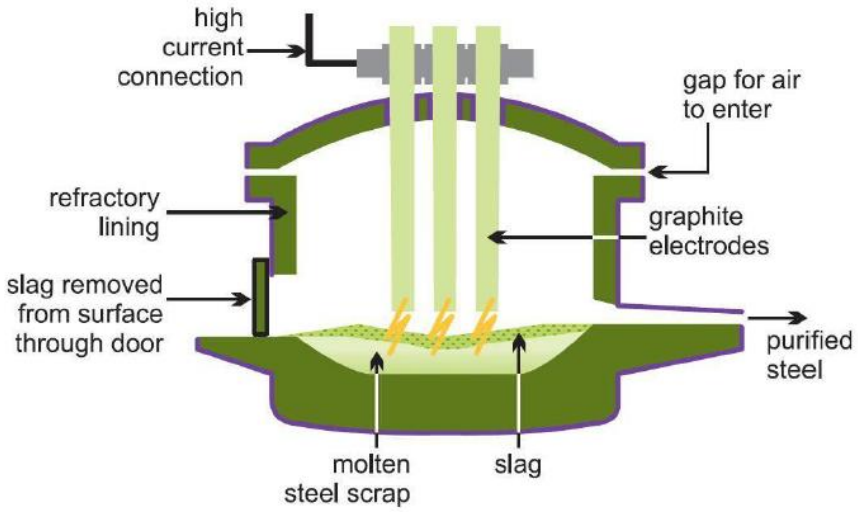

Figure 2.3: Electric Arc Furnace (EUMERCI, 2020)

Over the long term, EAF steelmaking process has potential that it possessed the advantages of low-capital investment, feeding recycled scrap metals, large reduction in specific energy and flexibility in varying production according to demand which balance out its slightly higher cost composition including raw materials in comparison to BOF steelmaking process. Although EAF steelmaking process utilizes scrap metals as feed, this does not consider as downside of it because if hot metals from blast furnace or direct-reduced iron is available, they can also be used as feed. Dramatic improvement to the EAF furnace design and operation are expected, particularly in reducing loss of energy.

2.2 Electric Arc Furnace Dust

EAFD is a solid waste generated in EAF steelmaking process, it is separated with the off-gas (gas sucked out from EAF) in direct evacuation system and taken to baghouse. Approximately 10-20 kg of EAFD is produced per tonne of steel, implying that 5-7 million tons of EAFD is generated every year globally (Al-Makhadmeh, et al., 2018). EAFD is known to contain heavy metals, for instance Pb, Cd, and Cr. As a result it is classified by European Waste Catalogue (EWC 2002) and United States Environmental Protection Agency (US EPA) as hazardous waste (Al-Makhadmeh, et al., 2018)

2.2.1 Dust Generation

Majority or in another word, 60% of the EAFD generation can be associated with CO bubbles bursting near arc and around slag surface (Tauriainen, 2015). CO bubbles mechanism generates two type of drops which are film drops and jet drops. Tauriainen (2015) stated that film drops are formed when the surface of liquid is broken by the approaching gas bubble while film drops are formed when the bubble cap disrupts and closes. Furthermore, film drops are generally small in size which enables them to travel with exhaust gas to form dust. In contrast, jet drops are larger and heavier than film drops and usually fall back to the furnace liquid bath.

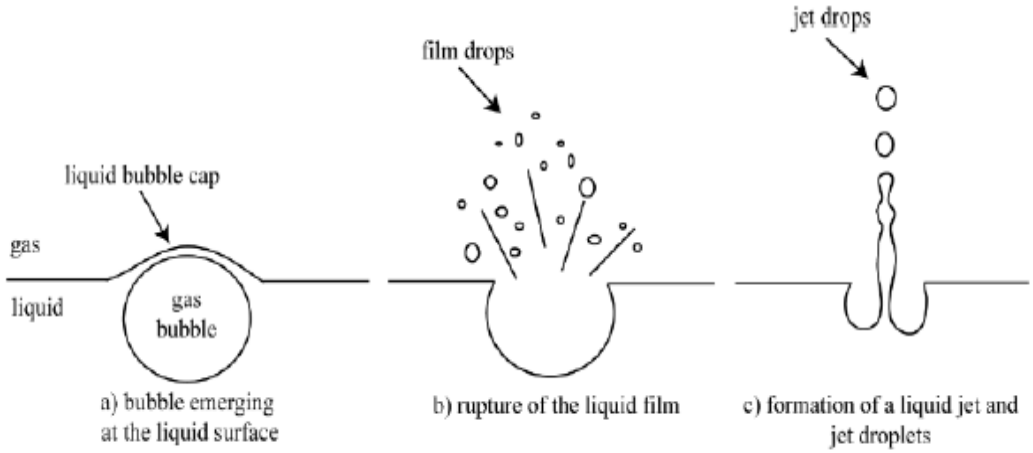

Figure 2.4 : Bubble Bursting in Liquid Surface (Tauriainen, 2015)

Other factors such as volatilisation, spreading of drops around zone of oxygen injection or arc and bursting of droplets within oxidising atmosphere also contribute to the formation of EAFD (Simonyan, Alpatova and Demidova, 2019). When the steel scrap is melted during the operation of EAF, EAFD forms as a result of the vaporisation of volatile metals such as Zn, Fe and Pb are condensed into vapour phase or mechanically carried over at the high processing temperature of the furnace (approximately 1600 ℃) and then being oxidised and cooled in the air flow (Sofilić, et al., 2004). EAFD is collected from the extensive dust collecting system that is attached to each furnace.

2.2.2 Dust Composition

Quantity and element composition of EAFD are different from plant to plant and mainly rely on type of scrap recycled, charging method, oxygen injection intensity,

mechanism of dust formation, operating temperature at different periods of melting and mechanism of dust formation (Simonyan, Alpatova and Demidova, 2019). Overall, EAFD composed of Zn, Fe, Pb, Ni, Mg, Mn, Cd, Cr, Si and S, mostly in the form of metal oxides but chlorides, sulphides, fluorides and sulphates could also be identified.

Table 2.1: Elemental Composition of EAFD in wt %. (Shawabkeh, 2010)

Element	wt %	Element	wt %
O	25.6	Mn	4.11
Mg	2.66	Fe	24.0
Al	0.52	Cu	0.25
Si	1.57	Zn	29.1
P	0.03	Ga	1.08
Si	0.34	Br	0.14
Cl	1.56	Cd	0.11
K	1.76	Sn	0.10
Ca	3.16	Sb	0.04
Ti	0.05	I	0.02
Cr	0.14	Pb	3.64

To enhance corrosion resistance and rust protection, steel has often gone through galvanisation, a process to apply a Zn coating on the steel. Increased use of galvanised steel in building construction and manufacturing of automobile has increased the zinc content in the EAFD, given the composition of EAFD is directly related to the type of scrap metal used. EAFD commonly contains 10-50 wt% of Zn which exists in the form of zincit (ZnO) and franklinite ($ZnFe_2O_4$) because of the reaction between Zn vapour and other gaseous compounds in the gas-cleaning system (Lee, et al., 2019). In recent years, there has been a rise in level of chlorine in EAFD because of the rise of Cl^- containing impurities particularly rubbers, polymers and paints in recycled scrap metal. After undergoing thermal destruction by the heat from EAF, these impurities are broken down to two parts, a part forms alkaline metal chloride from reaction with EAFD, another part is released in simple gaseous compound form of HCL or Cl_2. De Buzin, Heck and Vilela (2017) stated that average of 5 wt% chlorine could be found in EAFD, making it the most abundant element after

zinc, iron and oxygen in EAFD. Fe mostly appears in the form of magnetite (Fe_3O_4) and in franklinite ($ZnFe_2O4$) in EAFD.

2.3 Zinc Oxide and Zinc Ferrite

ZnO is the most widely used zinc compound. In terms of cosmetic and personal care products, it is manufactured as baby lotions, nail products and sunscreen products. Besides, it is used as catalyst in the vulcanization of rubber. Other than these, usages of ZnO are also employed in many processed and products including ceramics, pharmaceuticals and paints. For ZnO which is in nanoparticle size, it is explored in the semiconductor industry due to its properties of 3.37ev energy gap and 60 meV exciton binding energy. Martín (2015) reported that mainly three ways of processes, which are French process (pyrometallurgical method), wet chemical process (hydrometallurgical method) and American process (pyrometallurgical method) that contribute to the production of 100,000 tones ZnO per year.

In the refining stage of BOF and EAF steelmaking processes, Zn is volatized at high temperature to combine with with Fe_2O_3 to form $ZnFe_2O_4$ in the baghouse at some operation modes, particularly oxygen lance blowing for scrap melting in EAF steelmaking. Tauriainen (2015) stated that the reactions between ZnO and Fe_2O_3 are stated as below:

At ZnO interface:

$$2Fe^{2+} + 3ZnO \rightarrow ZnFe_2O_4 + 2Zn^{2+} \quad (2.6)$$

At Fe_2O_3 interface:

$$3Fe_2O_2 + 2Zn^{2+} \rightarrow 2ZnFe_2O_4 + 2Fe^{2+} + 5O_2 \quad (2.7)$$

Lately, $ZnFe_2O_4$ was determined to be a promising semiconductor photocatalyst because of its ability to absorb visible light and excellent photochemical stability. Overall, $ZnFe_2O_4$ is used in a wide diversity of technical applications , for instance magnetic materials, hot-gas desulphurisation and gas sensors (Tauriainen, 2015). $ZnFe_2O_4$ has a very stable spinel structure with A cations at octahedral interstices and B cations at the tetrahedral interstices.

Many literatures have provided important insight that higher content of $ZnFe_2O_4$ in the EAFD is known to make extraction of Zn and Fe more difficult, hence

leaching lixiviant which can effectively break down $ZnFe_2O_4$ is preferably selected for this study.

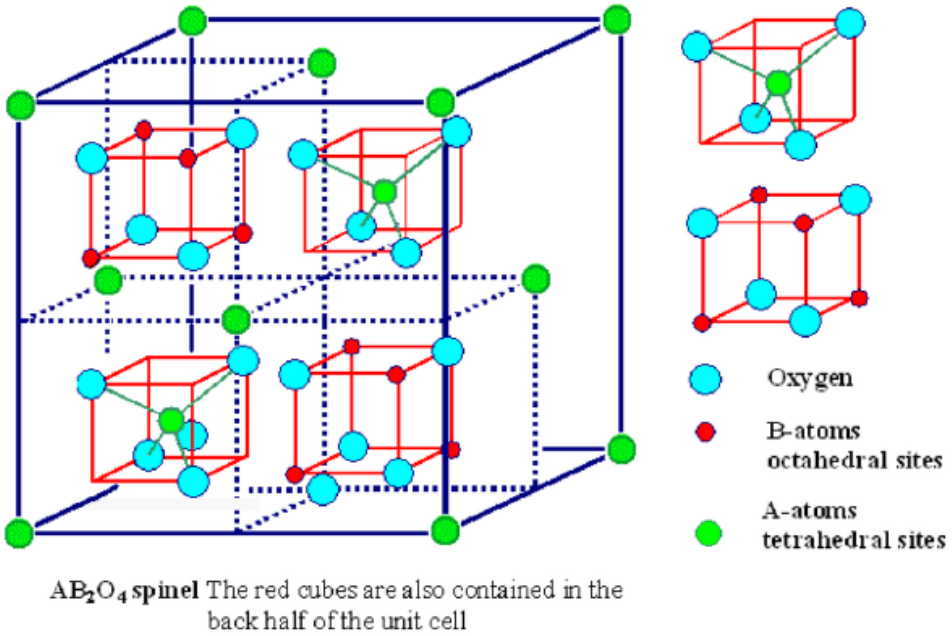

Figure 2.5: Spinel Structure (Tauriainen, 2015)

2.4 Pyrometallurgy

Pyrometallurgy methods are the pioneer in the recycling of EAFD, in other words they are the first method that has reached the commercialization. Pyrometallurgy methods include Waelz kiln process, rotary hearth furnace process, Ausmelt process and Plasma process. The purpose of pyrometallurgy is to recycle EAFD to produce crude ZnO, but these low-grade intermediate products have little commercial value, thus hydrometallurgy is needed to further process them (Tauriainen, 2015).

Waelz kiln process is the oldest and widely used pyrometallurgy method, the EAFD processed takes into account for almost 75% of the total EAFD treated worldwide and the Zn produced responsible for 5.2% of the refined zinc production globally (Julieth, et al., 2018). Firstly, a homogenous mixture (EAFD + flux + reductant) are pelletized as the load might swept away by kiln gas, and then the pelletized mixture is fed into Waelz kiln for drying and preheating by kiln gas (Martín, 2015). In the reaction zone (kiln), the metal oxides are reduced in the temperature of 1200 ℃, and due to this low temperature and addition of flux, Waelz kiln generates lower Fe metallization and lesser Zn dezinfication compared to rotary hearth furnace.

During the process, Pb and Zn are highly volatilised and then oxidised again as Waelz oxide in the outlet end (Martín, 2015). On the other hand, Fe is oxidised to form iron slag or Waelz slag. The dust off-gas undergoes purification in the off-gas treatment and finally, the EAFD which has been converted into Waelz oxide, are transferred to refineries to extract the metallic Zn (Julieth, et al., 2018). The primary shortcoming of Waelz kiln is the high amount of Waelz oxide and Waelz slag produced, meaning that there is a large number of remaining Zn, Pb and Fe (Lin, et al., 2017).

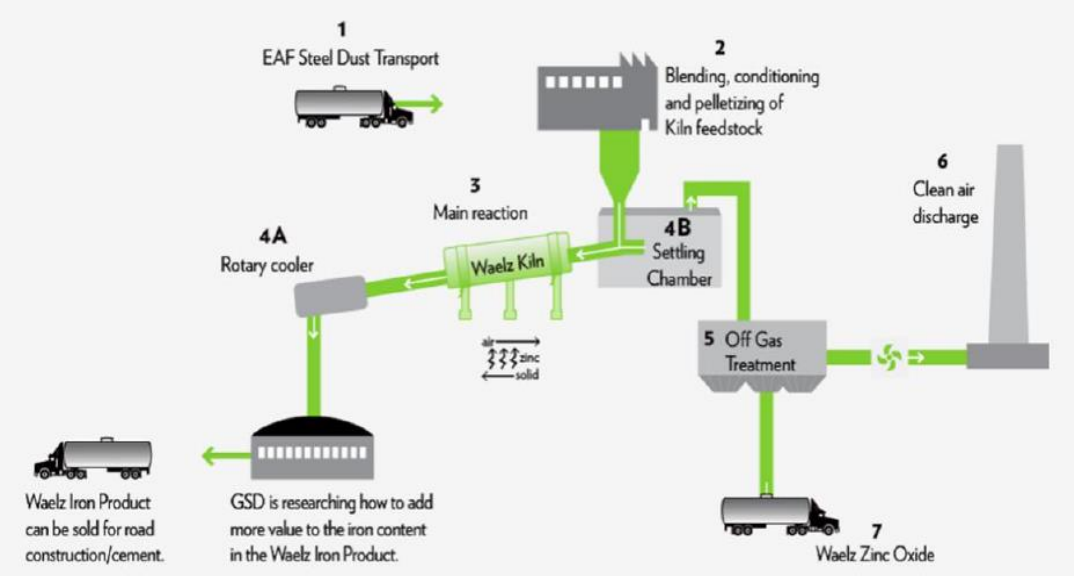

Figure 2.6: General Scheme of Waelz kiln Process (Julieth, et al., 2018)

2.5 Hydrometallurgy

Hydrometallurgical method is gaining importance for EAFD treatment among metallurgical industries due to the depletion of high-grade ores and valuable metallic values from EAFD. Recovery of Zn and Fe from EAFD can be processed through pyrometallurgical methods, hydrometallurgical methods and combined methods. Recently hydrometallurgical methods have emerged as an interesting alternative as they can fit on small scale, consume less energy, offer environmental benefits, operate in lower cost and provide higher flexibility (Teo, et al., 2018). Hydrometallurgical methods are generally based on acid and alkaline leaching. Acid leaching uses lixiviant such as H_2SO_4, HCl whereas alkaline leaching uses lixiviant such as NaOH and NH_4OH. There are currently two hydrometallurgical industrial processes, which are known as Ezinex and Zincex. Ezinex process includes ammonia leaching of dust, purification based on cementation and zinc separation via electrolysis (Palimąka, et al.,

2018). On the other hand, Zincex involves atmospheric leaching of dust using H_2SO_4, solvent extraction and electrowinning to recover Zn ingots (Palimąka, et al., 2018). The main downside of hydrometallurgical method is the presence of 50% of total zinc in the form of $ZnFe_2O_4$ of the total EAFD as $ZnFe_2O_4$ exhibits the strong stability through high percentage of covalent bonds within its tetrahedra and closely allocated oxygen ions (Al-Makhadmeh, et al., 2018).

2.5.1 Acidic Leaching

Until now, in acidic leaching, the attention in researches has been mainly focused to H_2SO_4 as leaching solution. Using H_2SO_4 offers benefits of modest price, high dissolution kinetics and capability to produce metallic Zn in low concentration when coupled with electrowinning process but jarosite ($KFe^{3+}{}_3(OH)_6(SO_4)_2$) which is harmful to the environment may form at pH < 2 (Al-Makhadmeh, et al., 2018). Moreover, it is also essential to control pH to prevent hydrolysis and precipitation of Zn $(OH)_2$. Havlik et al. (2005) performed leaching experiment using 0.4M H_2SO_4 with various acid-to-dust ratio (0.4, 0.6 and 1.2) at different temperatures (20, 40, 60, and 80 ℃). The result showed the increase of acid-to-dust ratio and temperature causes the increase of the Zn and Fe yield. The highest extraction of Zn is 67% obtained at 80 ℃ in a time of 1 hour, whereas the extraction of Fe is not ideal, with a yield of lesser than 10 %. The hydrometallurgical recovery of Zn from EAFD is proven to be feasible with comparatively high Zn yield, but majority of Fe in EAFD still remains in solid state.

Conversely, according to Teo, et al. (2018), HCl has been found to be an effective lixiviant for the leaching of EAFD, while avoiding the formation of jarosite, CL^- ions are helpful in dissolution of Zn and Fe as well as removing toxic elements, such as Cd and Pb from the dust as soluble chlorides. Furthermore, filtration technique applied using solid-liquid separation is easier in HCl leaching (Teo, et al., 2018).

2.5.2 Alkaline Leaching

The primary advantage of alkaline leaching is its selectivity towards Zn compared to Fe compounds, thus obtains Fe-free solution and practically eliminate complicated Fe removal process from electrolyte (Stefanova, et al., 2014). Nonetheless, it also has the disadvantage of needing high concentration of leaching lixiviant in order to obtain high zinc leaching efficiency, less economic compared to acid leaching and difficulty of solution recovery (Palimąka, et al., 2018). Palimąka, et al. (2018) revealed that the

maximum Zn extraction (88%) from EAFD was obtained using 6M NaOH, liquid / solid ratio (L/S) = 40 at 80 ℃ in their studies on Zn recovery from EAFD by hydrometallurgical methods by manipulating the variable parameters as summarised in Table 2.2.

Table 2.2: Parameter values for NaOH leaching of EAFD (Palimąka, et al., 2018)

Parameters	Value
NaOH Concentration, M	2, 4, 6
Temperature, ℃	20, 50, 80
Liquid-solid ratio, cm^3 / g	10, 20, 30, 40
Stirring speed, rpm	400
Time, min	120

XRD analyses performed on EAFD before and after leaching in (4M NaOH and 6M NaOH, at 80 ℃, L/S = 40), disclosed that the virtually all of Zn, in the form of ZnO from residue of (4M NaOH, 80℃, L/S = 40) had been removed. The efficiency increased slightly when increasing the concentration of NaOH from 4M to 6M. The dissolution of franklinite, $ZnFe_2O_4$ was suggested due to its decreasing peak intensity from EAFD before leaching to EAFD after leaching, even though the dissolution process is slow. Selectivity of Zn extraction using NaOH solution was proven with Zn concentration of 15190 mg / dm^3, while the concentrations of other metal elements were generally lower than 49mg /dm^3.

2.6 Extraction of Zn and Fe with HCl

For the leaching of $ZnFe_2O_4$ in EAFD using HCl, the acid attack process can be described as chemical equations below which occur simultaneously.

$$ZnFe_2O_4\,(s) + 2HCl(aq) \rightarrow ZnCl_2(aq) + Fe_2O_3(s) + H_2O(l) \qquad (2.8)$$

$$ZnFe_2O_4\,(s) + 8HCl(aq) \rightarrow ZnCl_2(aq) + Fe_2Cl_3(s) + 4H_2O(l) \qquad (2.9)$$

Notably, Fe compounds such as magnetite (Fe_3O_4) and hematite (Fe_2O_4) showed no acid solubility under leaching, proposing that the leaching of Fe is mostly come from dissolution of $ZnFe_2O_4$ (Lee, et al., 2019).

Various literatures reported that several factors such as temperature, acid concentration, pH and dust-to-acid ratio affect the extraction of Zn and Fe. When the temperature and HCl concentration increases, the amount of Zn and Fe extraction increases, but depending on HCl concentration, incremental in temperature exceeding an optimum temperature may lead to a decrease in Zn and Fe extraction. The increase in HCl concentration increases the amount of Cl-ions which are strong activator to dissolve Zn and Fe in EAFD. Teo, et al. (2018) suggested that Zn and Fe extraction demonstrate decrement at elevated temperature (80 ℃ - 90 ℃) in 3M and 5M HCl concentration, but demonstrate increment at elevated temperature for 1M HCl concentration. Lee, et al. (2019) reported similar result that if using H_2SO_4, under conditions (liquid-to-solid ratio = 3, temperature = 20 ℃, leaching time =30 minutes), when the acid concentration increased from 0.1 to 1.4M, , the leaching rate of Zn increases dramatically from 5.8% to 92% and finally reached the leaching rate of more than 97% at 3M. However, before reaching to 1.4M acid concentration, Fe was not dissolved, and even under strong acid condition (3.0M), the leaching rate was low (~10%).

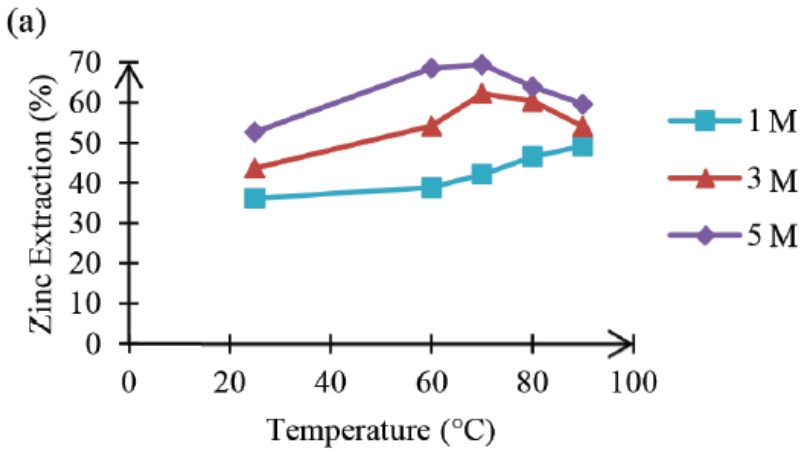

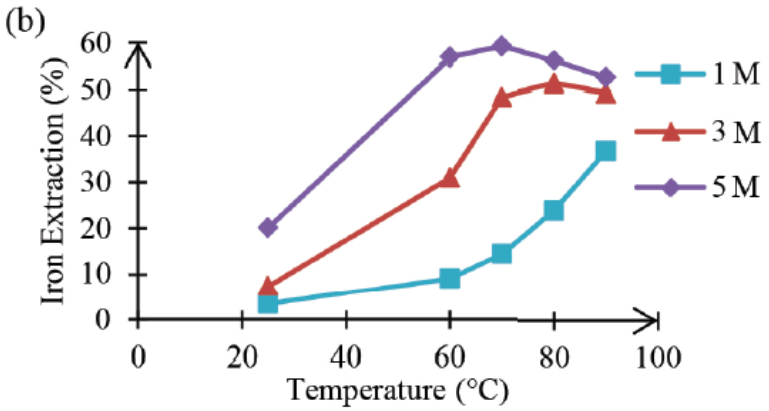

Figure 2.7: The Effect of HCl Concentration and Temperature on the Extraction of Zn (a) and Fe (b) (Teo, et al., 2018)

During the leaching reaction, pH is an important factor affecting the extraction of Zn and Fe as it can be monitored to maximize Zn extraction while minimize Fe dissolution. According to Lee, et al. (2019), a pH of > 4.5 ensured maximum extraction of Zn with minimum Fe dissolution irrespective of the properties in EAFDs and the acid type used. In the scope of the effect of dust-to-acid ratio, Teo, et al. (2017) stated in results that by increasing 1g to 8g of EAFD per 100 ml of HCl at 70 ℃ , the highest extraction of Zn and Fe, which is around 70% and 60% respectively, was observed at 3g of EAFD per 100 ml of HCl. Reduction in extraction of Zn and Fe was observed when further increase the amount of EAFD with constant volume of HCl. This could be explained by decrease in available HCl to extract Zn and Fe.

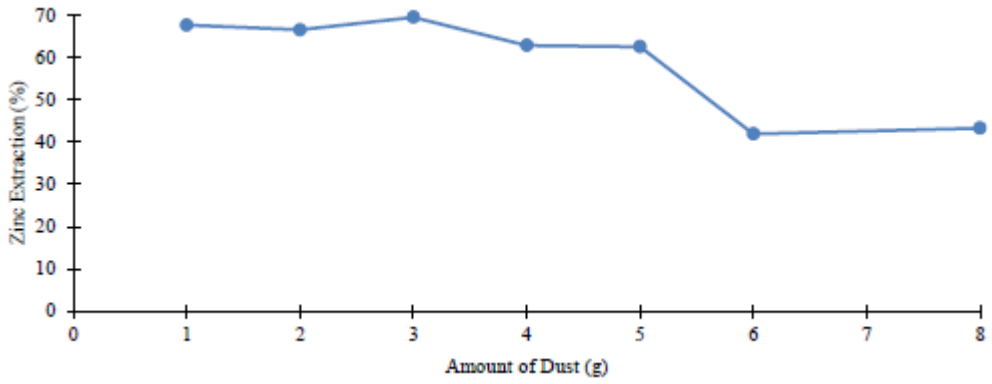

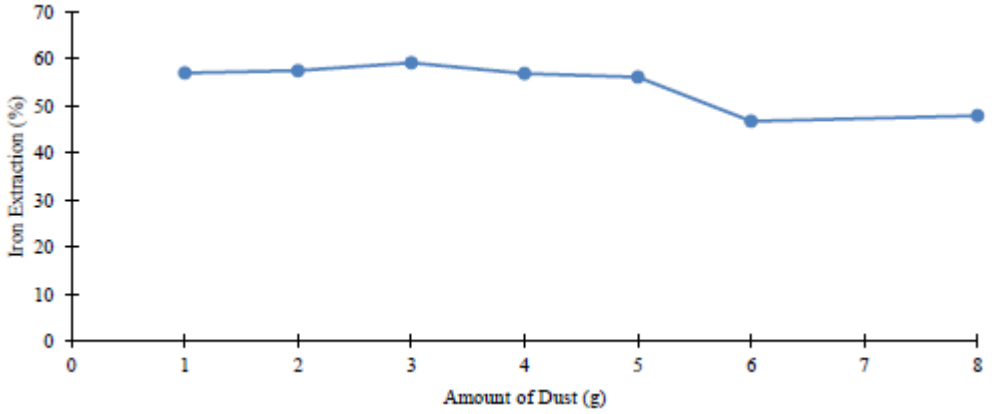

Figure 2.8: The Effect of Dust-to-Acid Ratio on (a) Zn and (b) Fe Extraction (Teo, et al., 2017)

Past experiments have provided comprehensive ideas that concentration, temperature, pH and dust-to-acid ratio are important factors for the extraction of Zn and Fe with HCl. Stirring speed does not considered as a significant factor.

2.7 Precipitation

Precipitation is a facile and common method to produce metal oxide. This method is utilised for simultaneous precipitation of more than one component from the aqueous solution. An alkaline solution such as NaOH is allowed to react with the metal precursors which are highly soluble inorganic salts in the form of chlorides, carbonates or nitrates to precipitate the metal hydroxide by starting to acidify the alkaline solution from acid solution by raising the pH value (Guwahati, 2014). The metal hydroxide will be subjecting to washing, centrifugation, drying and calcination to form the metal oxide. The solid formed is called ‘precipitate’ while the remaining liquid above the solid is called ‘supernatant’.

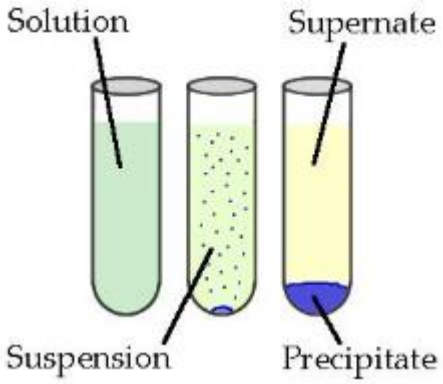

Figure 2.9: Formation of Precipitate in a Solution (Schaffer and Herman, 2019)

The reaction of precipitation displays several characteristics. First and foremost, the products formed are generally insoluble species in supersaturation condition. Afterwards, nucleation process creates numerous amounts of small particles, also known as nuclei. Afterwards, secondary processes like Ostwald Ripening and Digestive Ripening take into effect and significantly affect the particle size, shape, morphology and properties of the products obtained. The supersaturation condition which is resulted from a chemical reaction helps to induce precipitation (Trunschke, 2011).

The advantages of coprecipitation are simple, rapid and energy efficient preparation method. This is due to the facts that coprecipitation can produce a large number of metal oxides in a relatively short time and also utilise low cost chemicals acted as precursors (Irfan, et al., 2014). Despite the advantages, there are also several drawbacks. One of the drawbacks is that appropriate precursors are needed as this method does not work efficiently if the precursors have different precipitation rate. Next, inhomogeneity might be caused by inadequate coprecipitation of different ions from the precursors (Trunschke, 2011).

2.71 Metal Oxide Formed by Varying pH

Various literatures have provided important hindsight that several metal oxides can be produced through precipitation method. Marwaha, et al., (2017) reported that MgO was prepared by dropping 0.2M NaOH to 1.06M magnesium chloride hexahydrate [$MgCl_2.6H_2O$] at 50 ℃ for 2 hours to obtain Mg $(OH)_2$ at pH 8. The obtained Mg $(OH)_2$ was then calcined at 500 ℃ for 5 hours to obtain MgO nanostructure. Wang, et al., (2018) reported that when $ZnCl_2$ aqueous solution with certain mole ratio of glycerol/ Zn^{2+} was added with NaOH dropwise to a final pH value of 12, a white emulsion was formed. The emulsion was washed with ethanol and water twice, and after drying at 80 ℃ in an oven, ZnO nanoparticles were obtained

Mohanraj and Sivakumar (2017) stated that the aqueous solution (pH = 2) which consists of 1.01g $FeCl_3$ (96%) and 4.08g $FeSO_4.7H_2O$ (99%) was added with NaOH until pH 9 and pH 12, where brown and black precipitates were formed. The precipitates were then centrifuged and rinsed for 3 times with distilled water and ethanol. At last, the obtained precipitates were dried for 1 hour at 120 ℃ to obtain tetragonal maghemite (γ-Fe_2O_3) and magnetite (Fe_3O_4). Farag (2015) reported that nickel oxide, NiO was synthesized when 0.385g of nickel (II) chloride hexahydrate,

$NiCl_2.6H_2O$ was dissolved in 250ml double-distilled water to achieve certain molar concentration at room temperature. Subsequently, the resulting solution was stirred magnetically for 40 minutes at 50 ℃ temperature and 10 ml NaOH with certain molar was added drop by drop until pH 8.

Although these studies were conducted using pure form of chlorides as precursors which are different with leaching solution that composed of many elements in chlorides form, they served as promising guidance for this research. Hence, it is possible to precipitate metal oxides with respective pH as shown as Table 2.3:

Table 2.3: Possible Precipitation of Metal Oxides at Each pH Values

Metal oxides	pH
NiO, MgO	8
γ-Fe_2O_3	9
Fe_3O_4, ZnO	12

2.8 Thermal Analysis of Ferrous Hydroxide

Pinto, Lanza and Lago（2019）investigated the controlled dehydration of ferrous hydroxide, $Fe(OH)_3$ to hematite, Fe_2O_3 in their work. $Fe(OH)_3$ was prepared by precipitating iron(III) nitrate nonahydrate by ammonium hydroxide at pH 9. $Fe(OH)_3$ was then heated at different temperatures (150 ℃, 200 ℃, 300 ℃ and 450 ℃) for 180 minutes in air atmosphere. The ferrous hydroxides were named according to their heated temperature respectively ($150Fe(OH)_3$, $200Fe(OH)_3$, $300Fe(OH)_3$ and $450Fe(OH)_3$). Pinto, Lanza and Lago（2019）also reported that when the $Fe(OH)_3$ was subjected to heating at 150 ℃, 200 ℃, 300 ℃ and 450 ℃, according to the heating temperature, $Fe(OH)_3$ will lose % O and % H demonstrated at the equation below.

$$Fe(OH)_3 \rightarrow FeO_x(OH)_y + H_2O \tag{2.10}$$

For example, at 150 ℃ and 450 ℃, the emprical formulae obtained for the $Fe(OH)_3$ sample were $FeO_{1.06}(OH)_{0.89}$ and $FeO_{1.43}(OH)_{0.14}$, indicating loss of % O and % H increases as temperature increases.

Figure 2.10 shows the XRD patterns for 150 $Fe(OH)_3$, 200 $Fe(OH)_3$, 300 $Fe(OH)_3$ and $450Fe(OH)_3$. Based on the XRD results, they claimed that 150 $Fe(OH)_3$

was amorphous , while for those samples which were treated at temperature higher than 150 ℃, there was presence of hematite and its crystallinity increased as temperature increased.

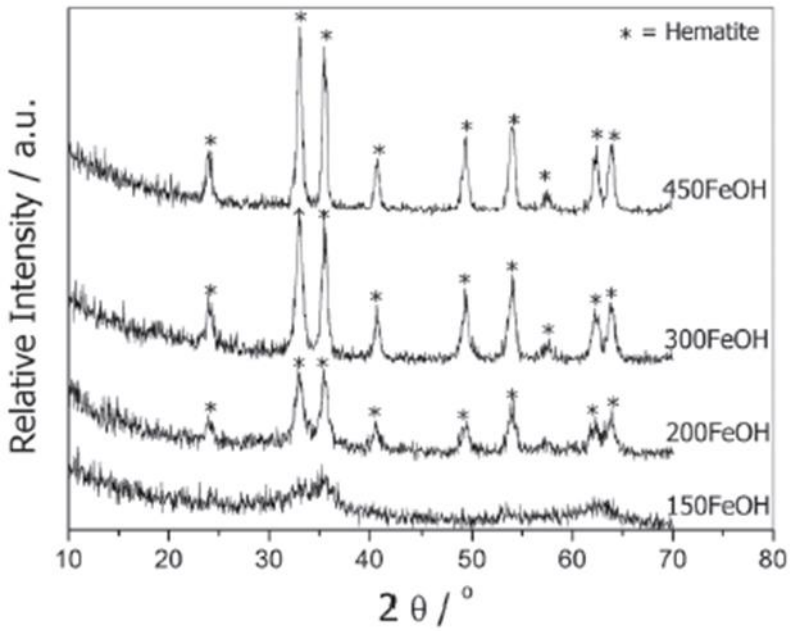

Figure 2.10: XRD Patterns for 150 $Fe(OH)_3$, 200 $Fe(OH)_3$, 300 $Fe(OH)_3$ and 450$Fe(OH)_3$ (Pinto, Lanza and Lago, 2019) *Noted that $Fe(OH)_3$ is named as FeOH in this work*

Pinto, Lanza and Lago（2019）stated there were two endothermic events demonstrated in their TGMS (Thermal Gravimetric Mass Spectrometry) curves, which are water loss between 100 ℃ and 200 ℃ and dehydroxylation at 234 ℃.

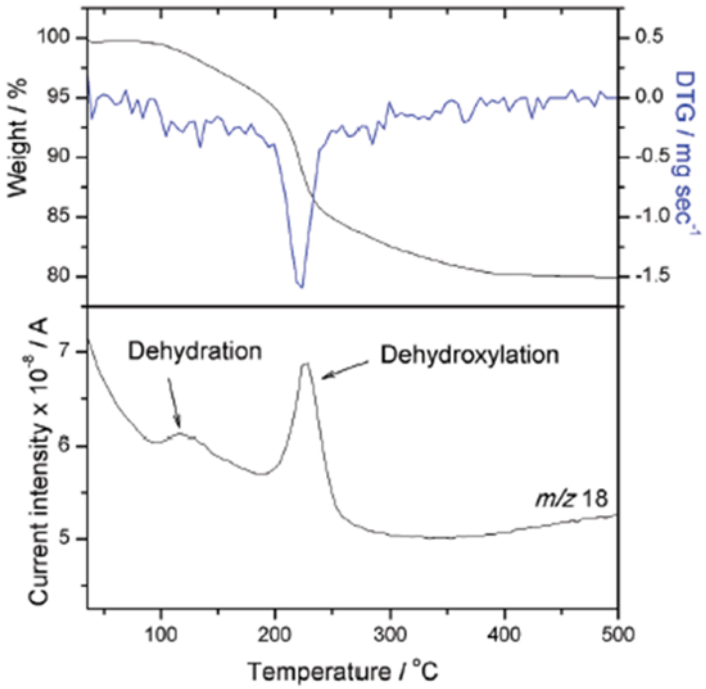

Figure 2.11: TGMS for the $Fe(OH)_3$ sample (Pinto, Lanza and Lago, 2019)

Besides, the SEM images of $Fe(OH)_3$ before heating (Figure 2.12) reported by Pinto, Lanza and Lago (2019) shows the irregular-shaped particles demonstrate agglomeration.

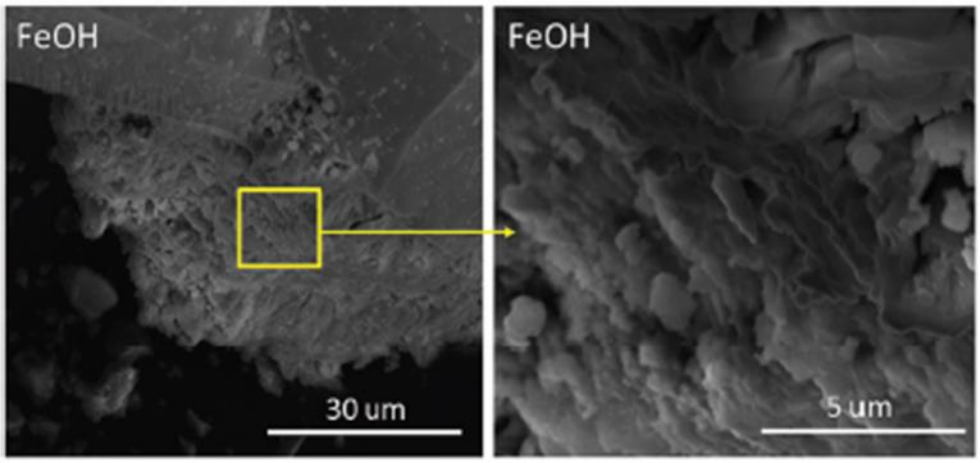

Figure 2.12: SEM images of $Fe(OH)_3$ (Pinto, Lanza and Lago, 2019)

2.9 Thermal analysis of Zinc Chloride Hydroxide Monohydrate

In the work performed by Moezzi, Cortie and Mcdonagh (2016), they examine the sequence of thermal transformation of zinc chloride hydroxide monohydrate, $Zn_5(OH)_8Cl_2 \cdot H_2O$ to crystalline zinc oxide, ZnO via thermal decomposition. TGA-

DTA curve in Figure 2.13 shows the first transformation of $Zn_5(OH)_8Cl_2{\cdot}H_2O$ occurred in the region of 100℃ - 161℃ when heated in air atmosphere.

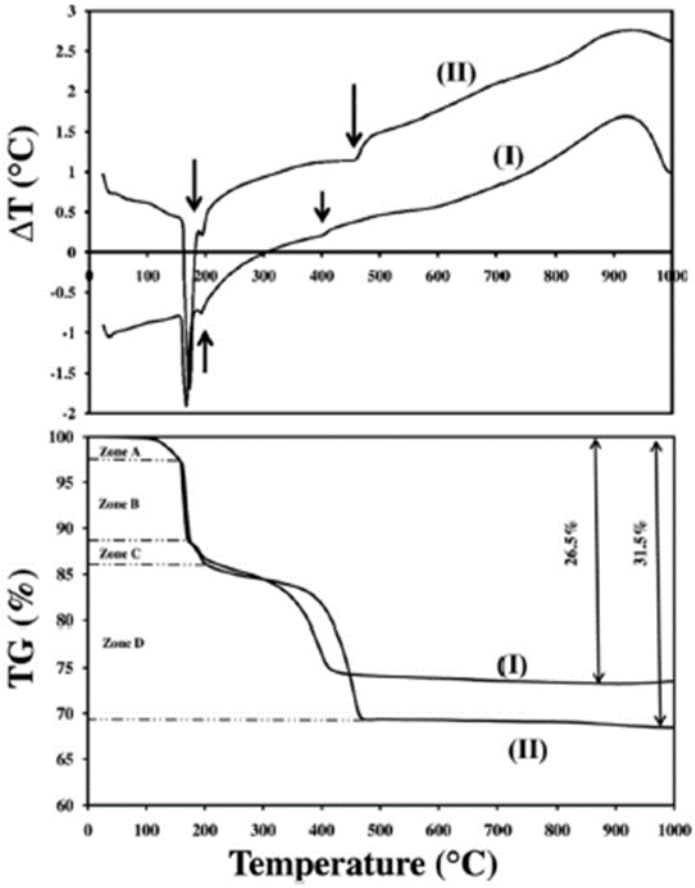

Figure 2.13: TGA-DTA of (I) freshly made $Zn_5(OH)_8Cl_2{\cdot}H_2O$ (II) $Zn_5(OH)_8Cl_2{\cdot}H_2O$ after 13 months aging (Moezzi, Cortie and Mcdonagh, 2016)

The process is related to dehydration process according to the equation below.

$$Zn_5(OH)_8Cl_2.H_2O_{(cr)} \rightarrow Zn_5(OH)_8Cl_{2(cr)} + H_2O_{(g)} \qquad (2.11)$$

The second transformation process occurred at the region in between 161℃ to 197℃, particularly with an endothermic peak demonstrating a decomposition at ~ 164℃.

$$Zn_5(OH)_8Cl_{2(cr)} \rightarrow 3ZnO + ZnO.ZnCl_2.2H_2O_{(cr)} + 2H_2O_{(g)} \qquad (2.12)$$

The third transformation process occurred at the region in between 197℃ to 225℃, which involves dehydration of $ZnO{\cdot}ZnCl_2{\cdot}2H_2O$ according to Equation 2.13.

$$ZnO.ZnCl_2.2H_2O_{(cr)} \rightarrow Zn(OH)_{2.}ZnCl_2 + H_2O_{(g)} \quad (2.13)$$

In the last stage of decomposition, ZnO is formed with the release of HCl at temperature > 400℃ according to Equation 2.14. The DTA shows one endothermic peak relating to this decomposition at ~400 °C.

$$Zn(OH)_{2.}ZnCl_2 \rightarrow 2ZnO + HCl_{(g)} \quad (2.14)$$

On the other hand, Gorodylova,et al., (2017) had prepared a review which summarized literature data regarding thermal transformation of $Zn_5(OH)_8Cl_2{\cdot}H_2O$. Particular attention was paid to the work performed by Rasines and Morales (1979), which studied the thermal decomposition of $Zn_5(OH)_8Cl_2{\cdot}H_2O$ in nitrogen atmosphere. In contrast with the previous work by Moezzi, Cortie and Mcdonagh (2016), in this work, the author revealed Zn(OH)Cl emerged as an additional intermediate compound due to the endothermic effect at 272℃.

Table 2.4: Thermal decomposition of $Zn_5(OH)_8Cl_2{\cdot}H_2O$ (Rasines and Morales,1979)

Process	Equation	T/℃	Mass loss (%)	Thermoanalytical effect/℃
Decomposition of $Zn_5(OH)_8Cl_2{\cdot}H_2O$	4.9	110-165	3.2	Endothermic /146
Decomposition of $Zn_5(OH)_8Cl_2$	5.0	165-210	9.9	Endothermic/202
Decomposition of Zn(OH)Cl	5.1	210-300	3.2	Endothermic/272
Volatilization of $ZnCl_2$	5.2	300-800	19.4	Endothermic/678

$$Zn_5(OH)_8Cl_2.H_2O \rightarrow Zn_5(OH)_8Cl_2 + H_2O \quad (2.15)$$

$$Zn_5(OH)_8Cl_2 \rightarrow 2Zn(OH)Cl + 3ZnO + 3H_2O \quad (2.16)$$

$$2Zn(OH)Cl \rightarrow ZnO + ZnCl_2 + H_2O \quad (2.17)$$

$$ZnCl_{2(l)} \rightarrow ZnCl_{2(g)} \quad (2.18)$$

Furthermore, the author revealed that the melting point of $ZnCl_2$ (275℃) was not detected, which should be overlapping with the decomposition of Zn(OH)Cl. Nevertheless, the boiling point of $ZnCl_2$ was detected at 678℃.

2.10 Summary

EAFD is a by-product from EAF steelmaking process and its hazardous nature encourages industries to extract valuable metal from it instead of disposing it in landfill. Hydrometallurgy method is more environmentally friendly compared to pyrometallurgy method in EAFD treatment. Specifically, HCl has been widely explored from literature reviews for being an effective leaching lixiviant of EAFD, demonstrating high Zn and Fe extraction amount. Various literatures have paved a way that different metal chlorides are able to be precipitated using NaOH at certain pH to form different solid metal hydroxides. The metal hydroxides are subsequently dried at high temperature to form solid metal oxides.

CHAPTER 3

METHODOLOGY AND WORK PLAN

3.1 Introduction

Various types of chemical, material, apparatus, equipment and instrument are required to conduct the whole experiment. Figure 3.1 summarizes the overall research methodology that can be separated into several sections which include leaching experiment, precipitation experiment and the analyses required.

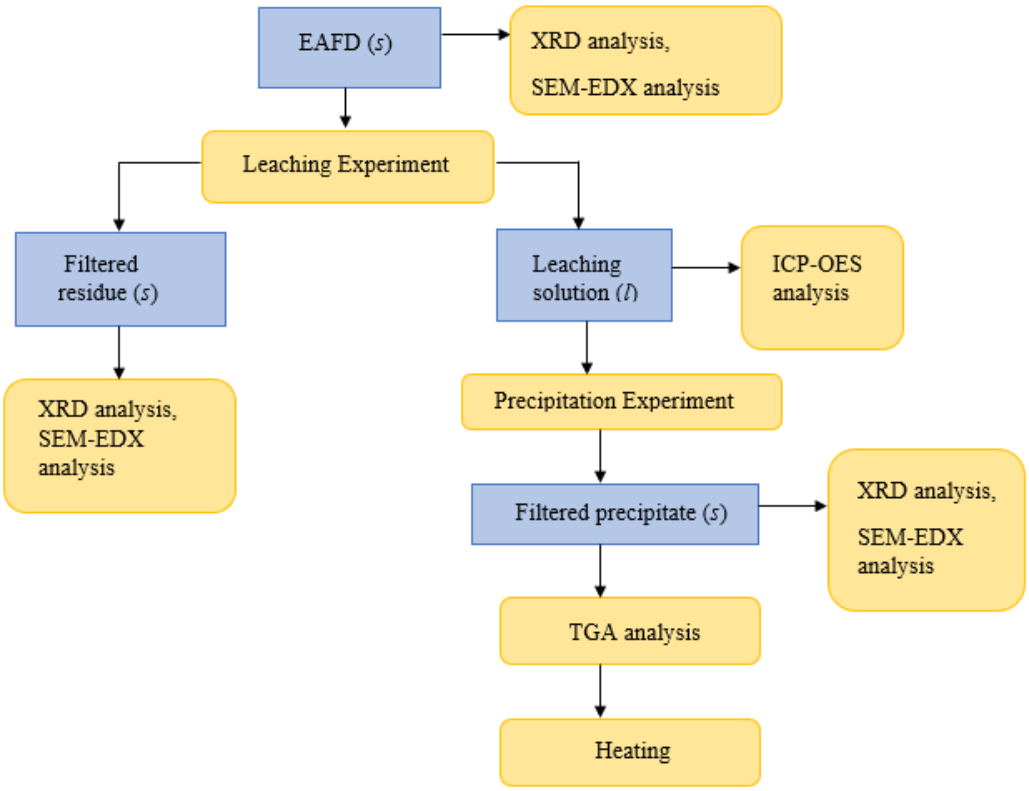

Figure 3.1: Overall Research Methodology

The phase composition of EAFD was first analyzed prior to the leaching experiment. XRD analysis was used to study the mineralogical composition of EAFD. SEM was conducted simultaneously with EDX to study the surface morphology and elemental composition of EAFD using SEM-EDX system. Afterwards, the leaching experiment was performed in atmospheric pressure using HCl. Meanwhile, the constant parameters include leaching time, leaching temperature, acid concentration, dust-to-acid ratio and stirring speed of the hotplate stirrer. Then the sample was filtered

out to separate the solid residue from the leaching solution. The solid residue was characterized with XRD and SEM-EDX, while the leaching solution was analyzed with ICP-OES to determine its Zn and Fe content.

The precipitation experiment was performed in atmospheric pressure and room temperature using NaOH. The fixed parameters include alkali concentration and stirring speed of the hotplate stirrer. Then the sample was filtered out to separate the precipitate from the precipitating solution. The precipitate was characterized with XRD and SEM-EDX. Finally, with the thermal decomposition temperature determined from TGA, the precipitate was heated to the required temperature.

3.2 Chemicals and Materials

The complete list of chemicals and materials needed with their source, estimated quantity and usage are shown in Table 3.1.

Table 3.1: Table of Chemicals and Materials

Chemicals / Materials	Source	Estimated quantity	Usage
EAFD	Outsource	100 g	Precursor for leaching process.
HCl	Fisher Scientific Sdn.Bhd	37%	Precursor for leaching process.
Zn standard solution	Merck	10 ml	For ICP-OES analysis.
Fe standard solution	Merck	10 ml	For ICP-OES analysis.
NaOH pellets	UTAR	-	To neutralize the acidity of the leaching solution in precipitation.
Deionized water	UTAR	-	To prepare diluted HCl solution and NaOH solution. To dilute standard

			solution and sample solution for ICP-OES.

3.3 Apparatus, Equipment and Instrument

The complete list of apparatus, equipment and instrument with their specification and usage are shown in Table 3.2.

Table 3.2: Table of Apparatus, Equipment and Instrument

Apparatus / Equipment / Instrument	Specification	Usage
Mortar and Pestle	-	To crush and grind EAFD into smaller form.
Test sieves	150 micron opening size	To separate finer EAFD from coarse EAFD.
Hot Plate (with magnetic stirrer)	IKA RCT basic	To heat up and stir the reacted mixture solution to desired temperature and rotational speed.
Thermometer	Alcohol-typed	To measure the temperature during leaching process.
Filter paper	Filtratech, quantitative filter papers grade QT45, 125mm diameter, 2-4um pore size	To filter out leached EAFD residue and precipitate.
Graham coil condenser	Favorit, 300mm, socket	To recycle the HCl fume back into HCl solution.
Conical flask (with plain still head, glass stopper)	500 ml	To connect Graham coil condenser in an enclosed system.

Plastic tubing	-	To channel water from fume hood to graham coil condenser.
pH paper	Merck, pH range 0 - 14	To measure the pH of the reacted mixture solution.
pH meter	-	To measure the pH of the reacted mixture solution.
Glass pipette and micropipette	-	Transfer a measure volume of solution
Burette	-	To drop NaOH into leaching solution.
Retort stand	-	To hold burette during precipitation.
Centrifuge tube	-	To contain sample solution and standard solution for ICP-OES. To keep solid residue and precipitate.
Scanning Electron Microscopy (SEM)	Hitachi Model S-3400N	To obtain the structure, crystallography, topography, chemical composition, morphology of EAFD and precipitate
Energy Dispersive X-Ray Spectroscopy (EDX)	Ametek	To perform elemental identification of EAFD and precipitate.
Inductively Coupled Optical Emission Spectrometry (ICP-OES)	Perkin-Elmer Optima 7000 DV	To perform analysis on the composition of EAFD.
X-Ray Diffraction (XRD)	Shimadzu Diffractometer Model XRD-6000	To perform characterization of EAFD and precipitate.

Thermo Gravimetric Analyzer (TGA)	Perkin Elmer STA 8000	To determine the thermal decomposition temperature of precipitate.
Tube Furnace	Lenton LTF 12	To heat precipitate at elevated temperature in an inert condition.

3.4 Leaching Experiment

The parameters of the leaching experiment were selected based on previous experiments done by other researchers such as Teo, et al. (2017) and Chong (2019). Dust-to-acid ratio of 1:30 was used. The experiment time was limited to 15 min. The solution in a 500 ml conical flask was immersed in a water bath at temperature of 50 ℃ and was stirred at 700 rpm by a magnetic hotplate stirrer. There are two purposes of utilizing Graham coil condenser in this experiment, which are forming a closed system to reduce vaporization amount of HCl and also condensing the released fume of HCl into HCl solution back by cooling it down. Coiled inner tube inside the condenser provides additional surface area for highly efficient cooling.

3.4.1 Procedures

First of all, the EAFD was crushed and grounded into finer form using pestle and mortar to reduce the dust size and remove agglomeration. Next, the EAFD was sieved to 150 μm size with test sieve. The purpose of crushing, grounding and sieving are for better leaching result. The EAFD was then dried in oven at a temperature of 80 ℃ for 2 hours to remove moisture.

Figure 3.2: EAFD

Figure 3.3: Evaporating Dishes Containing EAFD Covered with Aluminium Foil for Uniform Heating in An Oven.

10M of HCl solution was prepared by diluting the concentrated HCl (37 % w/w) with deionized water. The required volume of stock acid and deionized water was calculated with formulas below. The density and molar weight are known as 1.2 $\frac{g}{ml}$ and 36.46 $\frac{g}{mol}$.

I. Calculate the mass of 2.5 L of solution.

$$Mass\ of\ solution = 2500\ ml\ \times\ 1.2\frac{g}{mol} = 3000\ g \quad (3.1)$$

II. Calculate the mass of HCl.

$$Mass\ of\ HCl = 37\ \%\ \times 3000g = 1110\ g \quad (3.2)$$

III. Calculate the moles of HCl.

$$Moles = 1110g\ of\ HCl\ \times \frac{1\ mol\ of\ HCl}{36.46g} = 30.44\ moles \quad (3.3)$$

IV. Calculate the molarity of HCl.

$$Molarity = \frac{moles\ of\ HCl}{litres\ of\ solution} = \frac{30.44\ moles}{2.5L} = 12.18\ M \quad (3.4)$$

V. Compute the required volume of stock solution for desired molarity of acid.

$$M_1V_1 = M_2V_2 \quad (3.5)$$

Where

M_1 = concentration of stock solution, mol/L

V_1 = volume of stock solution, mL

M_2 = Concentration of diluted solution, mol/L

V_2 = volume of diluted solution, mL

The desired diluted acid is of 300mL and 10M, then the required volume of stock acid of 12.18 M is 246.31 mL:

$$V_1 = \frac{M_2V_2}{M_1}$$

$$V_1 = \frac{10\ M\ (300\ mL)}{12.18\ M}$$

$$V_1 = 246.31\ mL$$

Calculate the amount of deionized water (V_{DW}) needed to mix with the stock solution (V_1) to get diluted HCl (V_2) of 10 M:

$$V_1 + V_{DW} = V_2$$
$$V_{DW} = V_2 - V_1$$
$$V_{DW} = 300\ mL - 246.31mL$$
$$V_{DW} = 53.69\ mL$$

On exposure to air at room temperature, HCl condenses into colourless, corrosive fume that releases pungent odour. Hence, the dilution of HCl and leaching experiment must be conducted inside a fume hood. Figure 3.4 shows the leaching experiment which involved a setup using Graham coil condenser where its vapour inlet was connected to a 500 ml conical flask (topped with glass stopper) and its vapour outlet was directed to a receiving 250 ml beaker. Acid-dust mixture immersed in water bath at the left was heated to 50 ℃ . The water that passed through the coolant inlet and coolant outlet cooled the HCl fume as it went through the inner coil of the condenser. There it became solution again and dripped into the receiving beaker at the right.

Figure 3.4: Leaching Experiment Setup

At the end of leaching experiment, the leaching solution was filtered with Filtratech grade QT45 quantitative filter paper in order to remove solid residues. The minimum specifications of the filter papers are at 4 μm in pore size to retain medium particle size (5-10 μm) and 125 mm in diameter. The pH value of the leaching solution was examined using pH paper or pH meter. The solid residue obtained was dried at 80 ℃ for 1 hour.

The leaching solution was proceeded to ICP-OES analysis, diluted with dilution factor of 100. The required volume of sample solution needed was found using the equation 3.5. The diluted leaching solution was poured into a 15 ml centrifuge tube. Each sample solution produces three readings in mg / L.

Moreover, different concentration of Zn and Fe (0ppm, 5 ppm, 10 ppm, 15 ppm and 25 ppm) standard solutions were prepared by diluting the 100 ppm of Zn and Fe stock solution using the Equation 3.5, but the concentration is in ppm unit.

The calibration curves of Zn and Fe were prepared by using the different concentration of Zn and Fe (0 ppm, 5 ppm, 10 ppm, 15 ppm and 25 ppm) solutions, analyzed by the instrument ICP-OES. The calibration summary of Zn is demonstrated in Appendix B Picture B-1. The calibration curve of Fe is illustrated in Appendix A Graph A-1. The R-squared correlation coefficients obtained for Zn and Fe are 0.999353 and 0.999303. This shows that the results obtained are accurate and reliable. On the other hand, the solid residues were studied using XRD and SEM-EDX to characterize it and compare with the raw EAFD.

3.5 Precipitation Experiment

The precipitation experiment setup consists basically of a burette, beaker and of a hotplate magnetic stirrer as shown at Figure 3.5.

Figure 3.5: Precipitation Experiment Setup

First, 0.5 M of NaOH solution was prepared by dissolving 0.8 g of NaOH pellets in 40 ml of deionized water in a 250 ml beaker. The mass of NaOH pellets required was calculated with Equation 3.6.

$$mass\ of\ NaOH = V \times MW_{NaOH} \times C \tag{3.6}$$

Where,

V= volume of the stock solution, L

MW_{NaOH} = molecular weight of NaOH, (g/mol)

C = concentration of the stock solution, L

$$mass\ of\ NaOH = 0.04\ \text{L} \times \frac{40\ g}{mol} \times 0.5 \frac{mol}{L}$$

$$= 0.8g$$

The 0.5M NaOH solution was poured into the burette and then clamped with a retort stand. When the burette was filled, an initial volume reading was taken. After that, the 0.5M NaOH solution was added dropwise to the 250 ml beaker containing 10 ml of the leaching solution under continual stirring of 400 rpm at room temperature. The pH of the solution in the beaker was closely monitored with a pH meter. The colour change of the solution was observed and recorded. Once there was any precipitate formed in the solution, the stopcock of burette was closed and the final volume reading was taken. Volume of NaOH solution consumed, or in other words, the difference in volume, was calculated by taking the difference of the final and initial volume reading. Noted that the burette is refilled with 0.5M NaOH solution when the endpoint of the burette was reached.

The precipitate formed was filtered and dried in an oven at 80 ℃ for 1 hour. This series of steps was repeated for the remaining solution until a final pH value of 14 was achieved. Similar with the solid residue in the leaching experiment, the precipitate formed was characterized with XRD and SEM-EDX. Approximately 20 mg of the precipitate was thermally analyzed with TGA to determine the thermal decomposition temperature, which is the elevated temperature where the thermal decomposition of material occurs in an inert atmosphere (absence of oxygen). Each precipitate was heated in a tube furnace according to thermal decomposition temperature found.

3.6 Inductively Coupled Plasma - Optical Emission Spectrometry (ICP-OES)

Inductively Coupled Plasma Optical Emission Spectrometry (ICP-OES) is a powerful analytical tool used for the detection and measurement of trace elements in various samples from a myriad of categories including biological, geological, metals, organic and environmental. The technique is based on the ionization of an analysis sample by radiofrequency-induced argon plasma.

The working principle of ICP-OES started with injecting a sample solution into a spray chamber through a nebulizer. The sample solution is then converted into aerosol and focused to the plasma central channel. The ICP-OES at its core sustains a high temperature of excitation force up to 10000 K that quickly vaporize the aerosol.

The elements of the sample are released as free atoms in gaseous state. The atoms obtain additional energy by greater collisional excitation within plasma and they are promoted from atoms to ions and finally to the excited states (Hagen & Sneddon 2009).

The excited atoms return to the ground states by releasing light emission. The separation of light emission into wavelengths is done through diffraction grating. Then, the wavelengths are converted to a measurable electrical signal by photomultiplier in the spectrometer. The content of each element is able to be determined by comparing the intensity of the electron signal to previous measured intensities of know concentration.

The wavelengths are 206.2 nm for Zn and 238.204 nm for Fe. The intensity was plotted against the concentration of standard solution. The calibration of R-squared correlation coefficients should be > 0.999 to ensure the reliability, accuracy and precision of the result.

3.7 X-Ray Diffraction (XRD)

XRD is used to characterize the crystalline material and provide details on crystallographic structure, crystallographic phase, preferred orientation of crystal and interatomic spacing. X-rays are formed via accelerating electron into a copper cathode and directing electrons to the target material. X-rays of multiple wavelengths which consist of K-alpha and K-beta are produced once the electrons have enough energy to remove themselves from material's inner electrons shell (Bunaciu, Udriştioiu & Aboul-Enein 2015). The electromagnetic wavelength, diffraction angle and spacing of the lattice for constructive interference can be discussed by Bragg's law.

$$n\lambda = 2dsin\theta \tag{3.7}$$

Where

n = order of reflection

λ = X-ray wavelength

d=spacing between crystal plane

θ= measuring angles

The crystal size effect observed in XRD peaks can be described by the Scherrer equation which relates crystal size to line width.

$$L = \frac{K\lambda}{\beta cos\theta} \tag{3.8}$$

Where

L = Dimension of the particle in the direction perpendicular to the reflecting plane

K = constant, often taken as 1

λ = X-ray wavelength

β = peak width

θ = angle between the beam and the normal on reflection plane.

3.8 Scanning Electron Microscopy with Energy Dispersive X-Ray Spectroscopy (SEM-EDX)

Scanning Electron Microscope (SEM) focuses electron beams on the sample to obtain the structure, crystallography, topography, chemical composition, morphology of sample from high resolution images at nanoscale (Nanakoudis,2015). Energy Dispersive X-Ray Spectroscopy (EDX) is used with SEM for performing elemental identification, chemical analysis and quantitative compositional information. X-rays generation in SEM is a two-stage process. Initially, the sample is bombarded by electron beam, exciting the electrons from the atoms to leave a lower energy shell to a higher energy shell, thus creating an electron hole. In the second stage, the electron hole which has a positive charge is filled by an electron from a higher energy shell. X-ray is emitted due to this energy difference.

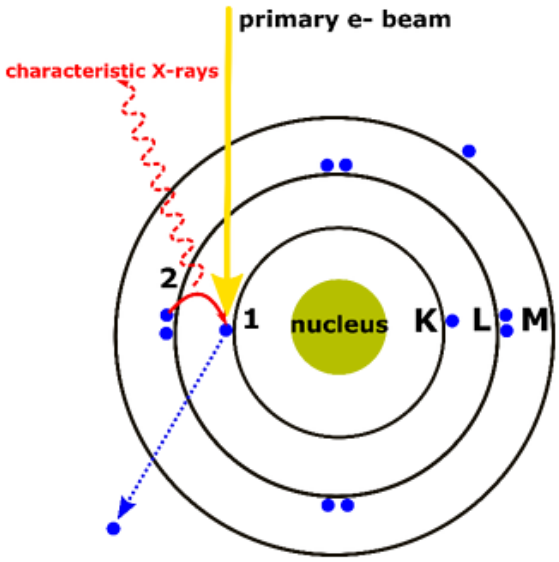

Figure 3.6: X-ray generation process (Nanakoudis, 2019)

An EDX detector measures the number of emitted X-rays versus their energy. The elemental composition of sample is determined by evaluating the energy of the X-rays emitted from the area being excited by electron beam. EDX can only provide surface elemental composition of the samples rather than bulk compositions.

3.9 Thermogravimetric analysis (TGA)

Thermogravimetric analysis is a technique of thermal analysis in which the weight of a sample is monitored and measured as a function of time as the temperature changes. It will be conducted for the precipitates using the settings and specifications of TGA shown in Table 3.3.

Table 3.3: TGA Setting and Specification

Setting	Specification
Crucible	Al_2O_3 crucible with pierced lid
Furnace Design	Vertical
Balance design	Top loading, single beam
Temperature Program	30℃ – 1000℃ with 10℃/min
Atmosphere	Nitrogen
Cooling time	60 min

Simultaneous analysis of TGA (thermogravimetry analysis), DTG (derivative thermogravimetry) and DTA (differential thermal analysis) results were interpreted with a single sample run. DTG is the differential weight (weight loss or weight increase) against time, whereas DTA is the differential temperature (temperature difference between the sample material and the reference material) against time or temperature.

3.10 Summary

In short, they are two main parts in this study which are leaching of EAFD and precipitation of leaching solution. The aims and objectives of this study are achieved when maximum extraction of Zn and Fe from EAFD, characterization of the composition and morphology of EAFD, as well as the formation of metal oxides are completed successfully.

CHAPTER 4

RESULTS AND DISCUSSION

4.1 Introduction

This chapter involves the presentation and discussion of results with reference to the aims and objectives. Firstly, the discussion commenced with the leaching experiment results. Subsequently, the results of characterization from various analysis techniques are discussed. The same goes for the precipitation experiment.

4.2 Leaching

Considering Zn and Fe are the main components of the dust in EAFD and the effectiveness of HCl in breaking the spinel structure of $ZnFe_2O_4$ as described by (Teo, et al., 2017), Zn in the form of zinc chloride ($ZnCl_2$) and Fe in the form of ferric chloride ($FeCl_3$) or in the form of ferrous chloride ($FeCl_2$) are expected to be obtained after the reaction. Figure 4.1 shows the leaching solution of 10M collected and stored in a Scott bottle after leaching and filtering.

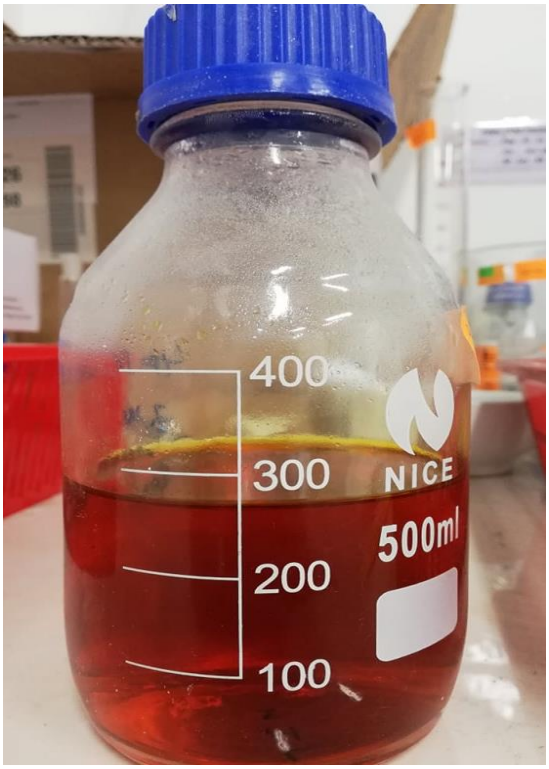

Figure 4.1: Filtered Leaching Solution of 10M

$FeCl_3$ in solution state appears as colourless to brown depending on the concentration whereas $ZnCl_2$ in solution state is a colourless solution (PubChem,n.d.). Therefore, the reddish-brown colour of the leaching solution indicates that the presence of high concentration of $FeCl_3$. The intensity of brown colour of $FeCl_3$ may be toned down by colourless $ZnCl_2$ and the remaining colourless HCl. At the same time, the observation provides clear evidence that $FeCl_2$ which is greenish in colour is unlikely to be found in the leaching solution.

In the aspect of recycling the HCl fume to HCl solution during leaching, despite the condensed HCl droplet formed at the inner wall of the conical flask and also at the vapour outlet as shown in Figure 4.2, it was observed that no condensed HCl dripped into the receiving beaker. The possible reason for this is a water solution containing 37wt% HCl boils at 57 °C, thus there was insufficient energy input to cause adequate and complete vaporization of the solution.

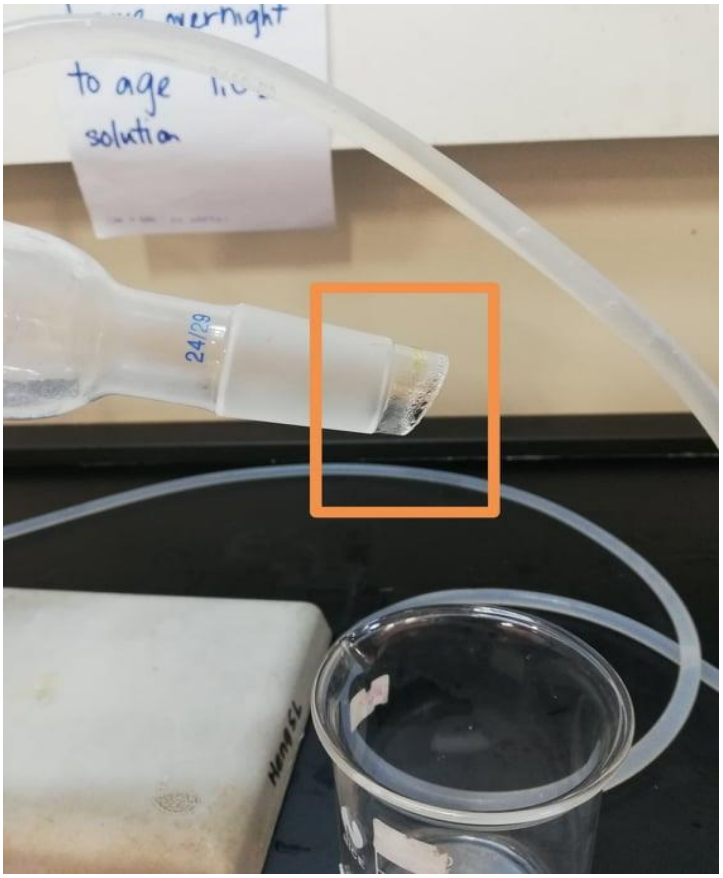

Figure 4.2: HCl Droplets at Vapour Outlet

4.2.1 Characterization of Leaching Solution Sample

The standard calibration curves for Zn and Fe were obtained with R-squared correlation coefficient of 0.999353and 0.999303 individually. The extraction amount obtained from the sample solution was shown at the Table 4.1.

Table 4.1: Dilution Factor and Extracted Amount of Zn and Fe

	Zn	Fe
Dilution factor	x 100	x 100
Extracted amount (mg/L)	69.26 mg/L	132.3 mg/L

The extraction percentage was calculated as below:

$$Extraction\ \% = \frac{Extracted\ amount\ \left(\frac{mg}{L}\right) \times Volume\ of\ Leaching\ Solution\ (L) \times Dilution\ Factor}{Weight\ of\ Element\ in\ EAFD\ (mg)} x\ 100\% \quad (4.1)$$

For Zn,

$$Extraction\ \% = \frac{\left(69.26\,\frac{\mathrm{mg}}{\mathrm{L}}\right) \times 0.3L\ \times 100}{2202mg} \times 100\% = 94.36\%$$

For Fe,

$$Extraction\ \% = \frac{\left(132.3\,\frac{mg}{L}\right) \times 0.3L\ \times 100}{4178mg} \times 100\% = 95.00\%$$

From the results, it can be deduced that the extraction percentages for Zn and Fe are close to that as commented by Chong (2019), which are 96.7% and 98.7% respectively in his work. To sum up, it is confirmed that in order to achieve extraction of Zn and Fe of more than 90%, the optimum condition of the HCl is to be performed at 10M and 50 ℃.

4.2.2 Characterization of EAFD Before Leaching

ICP-OES analyses shows that the average Zn and Fe content were ~22wt% and 42wt%, respectively. The XRD diffraction pattern of the EAFD is showed in Figure 4.3. The

XRD diffraction pattern proves the presence of Zn in the form of zincite, ZnO, and in the ferritic form as zinc ferrite, $ZnFe_2O_4$. Fe occurred in as already mentioned zinc ferrite and in oxide form as magnetite, Fe_3O_4.

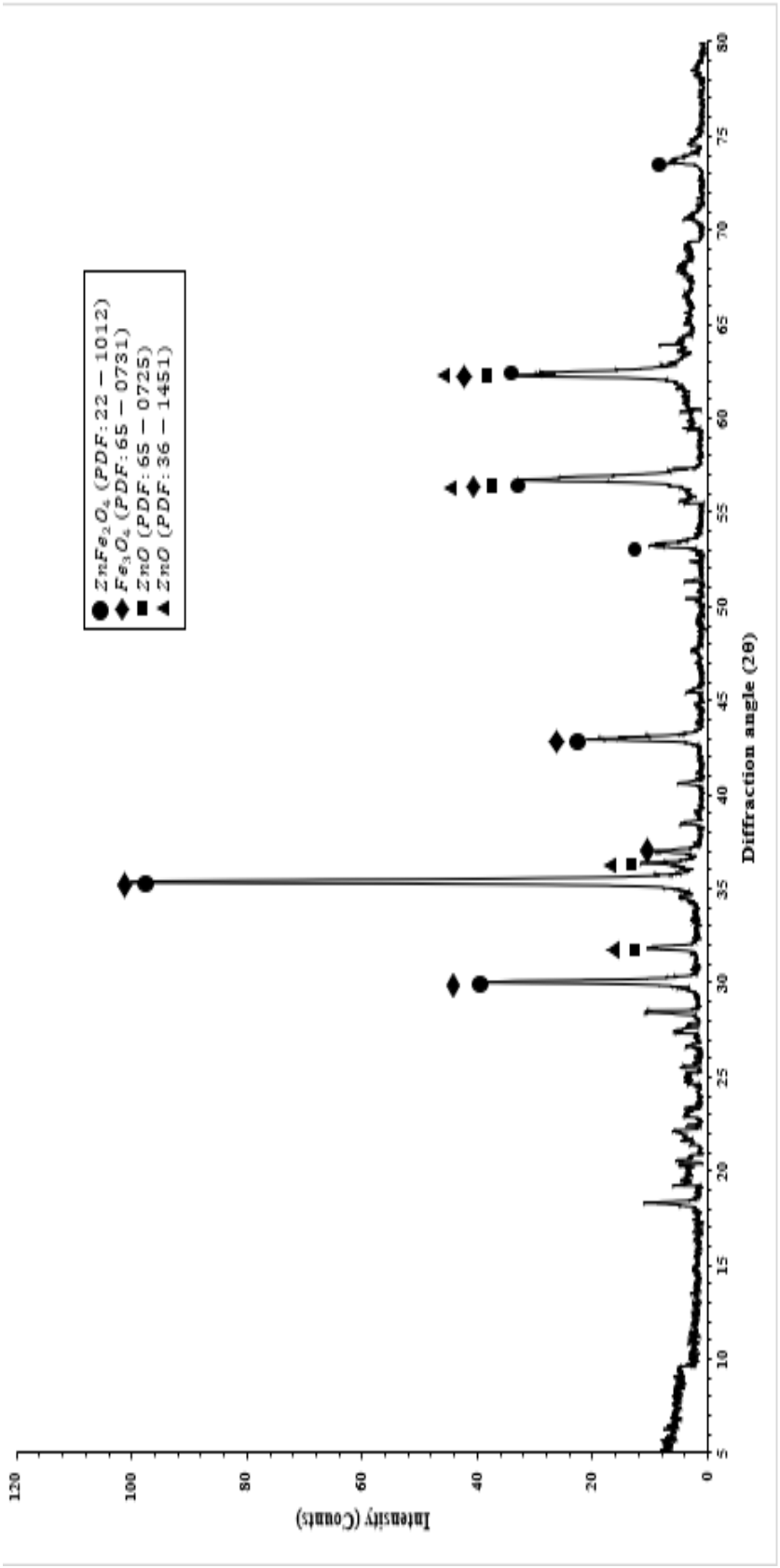

Figure 4.3: XRD Pattern of EAFD

SEM images of the EAFD are showed in Figure 4.4 and Figure 4.5. The morphology from both figures show that the EAFD consists of two main fractions (coarse and fine spherical particles), where agglomerates are created by fine particles covering big particles.

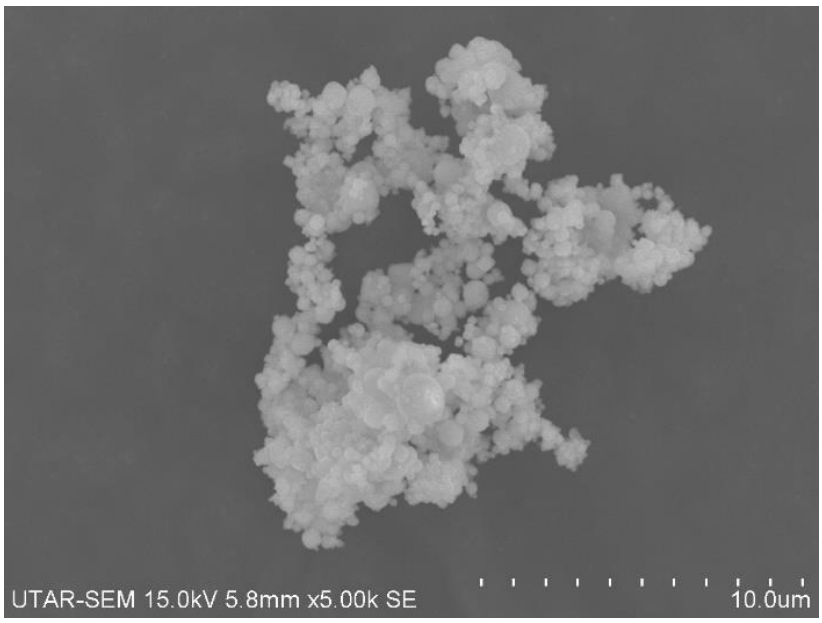

Figure 4.4: SEM Image of EAFD at 5k Magnification

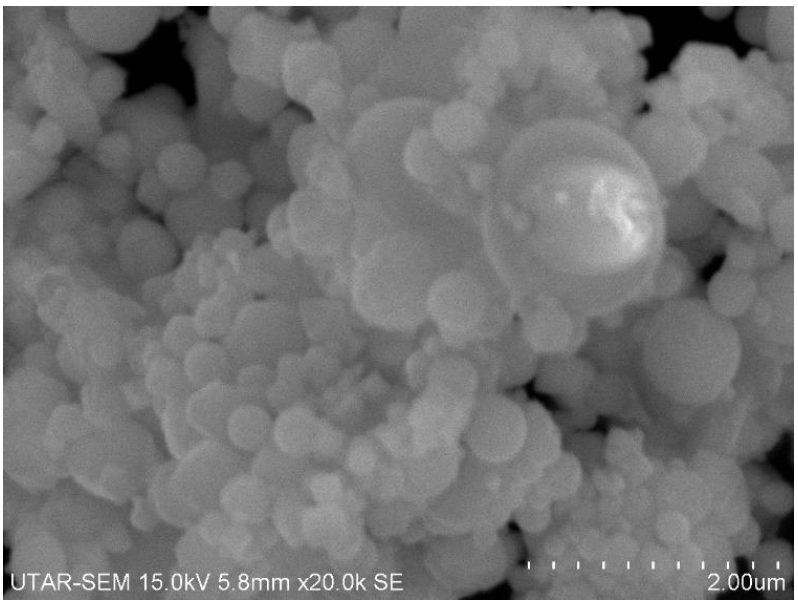

Figure 4.5: SEM Image of EAFD at 20k Magnification

EDX result from Figure 4.6 presents the elemental analysis result for the EAFD. It is noted that carbon (C), oxygen (O), zinc (Zn) and iron (Fe) are the dominant elements of EAFD.

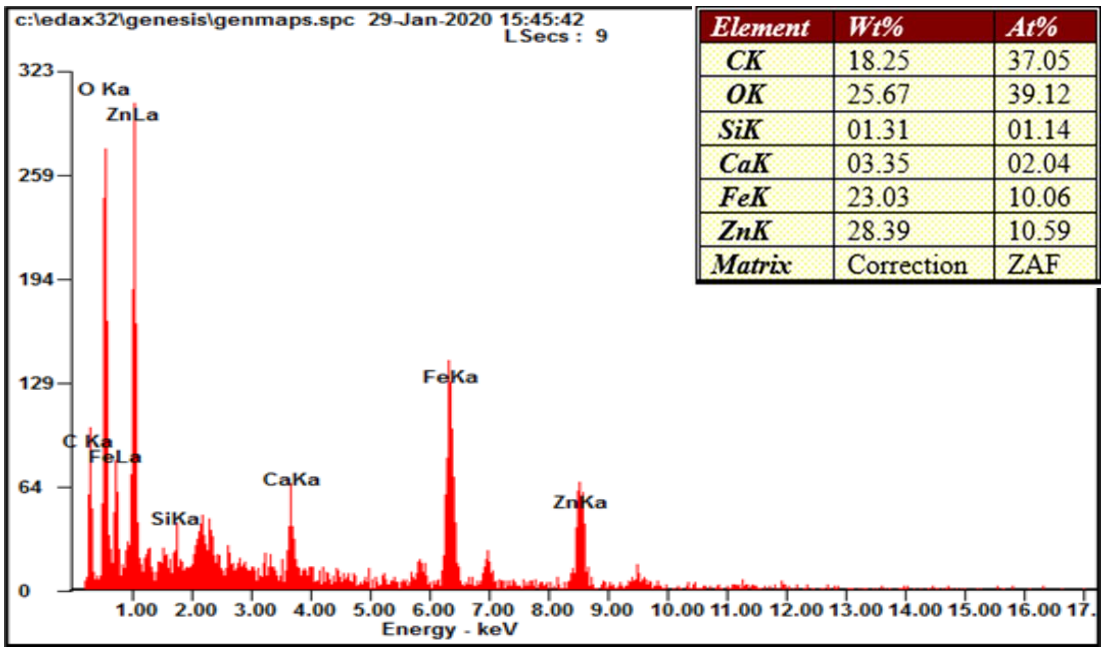

Element	Wt%	At%
CK	18.25	37.05
OK	25.67	39.12
SiK	01.31	01.14
CaK	03.35	02.04
FeK	23.03	10.06
ZnK	28.39	10.59
Matrix	Correction	ZAF

Figure 4.6: EDX Analysis of EAFD

4.2.3 Characterization of Solid Residue After Leaching

After filtering and drying at 80 ℃ for 1 hour, the colour of the solid residue was observed prior to scrapping it off and kept in a 15 ml centrifuge tube. Figure 4.7 shows that the solid residue is black in appearance. It is possible to speculate the black solid residue is the carbon that cannot be leached throughout the experiment. This is due to the fact that at standard pressure and temperature, carbon does not dissolve in any acids. It will only react with hot concentrated oxidizing acids especially nitric acid to form mellitic acid.

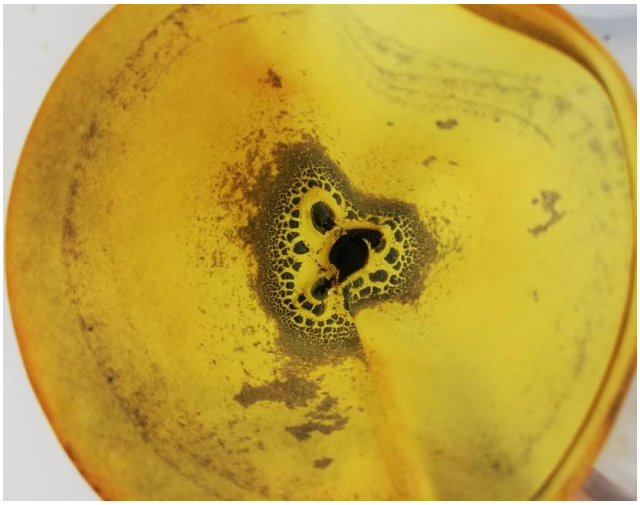

Figure 4.7: Solid Residue from 10M Leaching

Evidence in favor of this explanation is found in the XRD pattern of the solid residue after leaching, presented in Figure 4.8, which identifies the presence of carbon. The peaks of $ZnFe_2O_4$, Fe_3O_4, ZnO are not observed after leaching. Noted that the peaks at $2\theta = 38.42°$, $44.72°$, $64.98°$, $78.14°$ suggest the presence of aluminium because of the aluminium-made sample holder subjected to X-ray qualitative diffraction analysis on an X-ray diffractometer together with the sample.

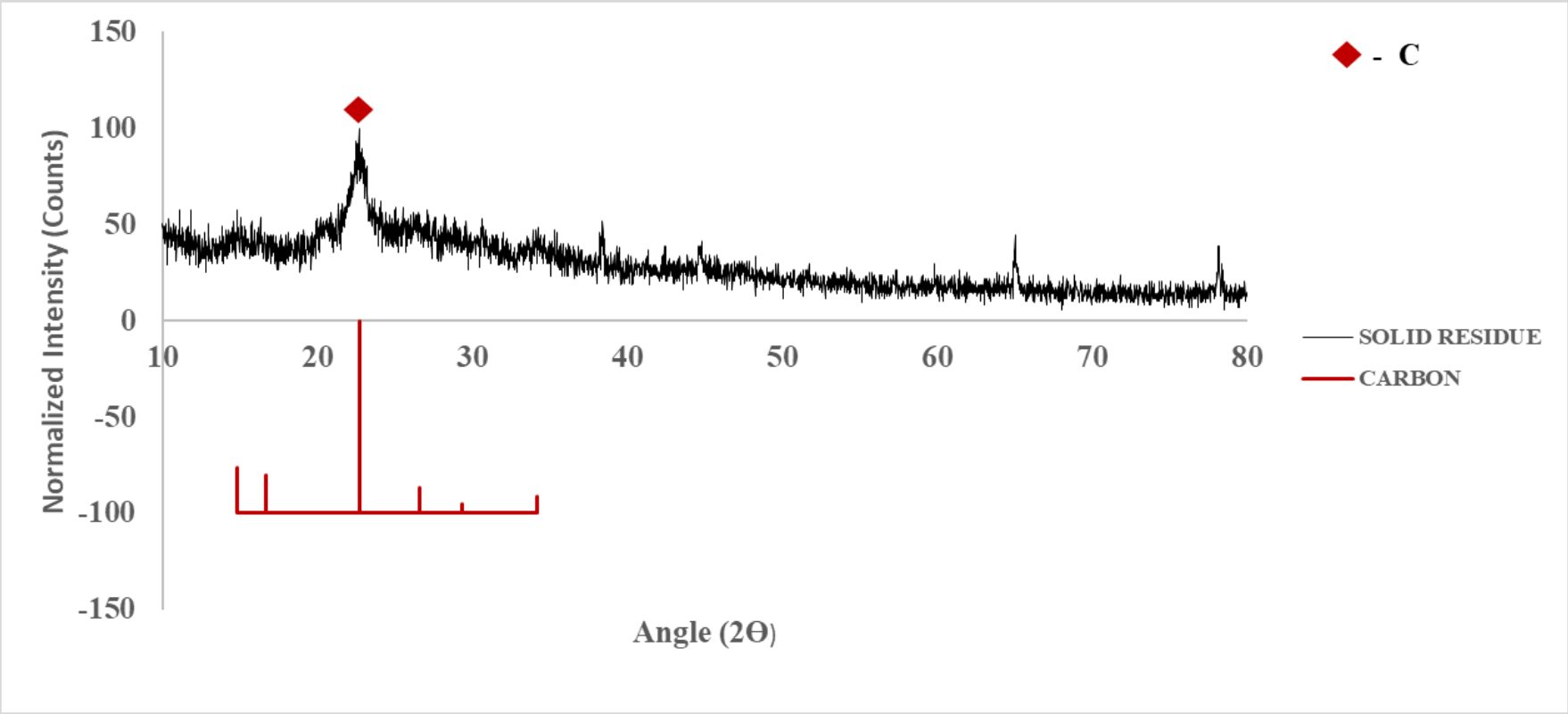

Figure 4.8: XRD Pattern of Solid Residue

As shown at Figure 4.9, carbon content is the highest among all elements, validating the black residues were probably carbon. Apart from that, it could be seen that the atomic percentage of silicon increased significantly from 1.14 at% to 10.82 at% after leaching, which revealed that silicon in the form of silicon dioxide, SiO_2 are not leachable by HCl since it does not react with most acids other than hydrofluoric acid. 4 at% of chloride particles are detected after the leaching.

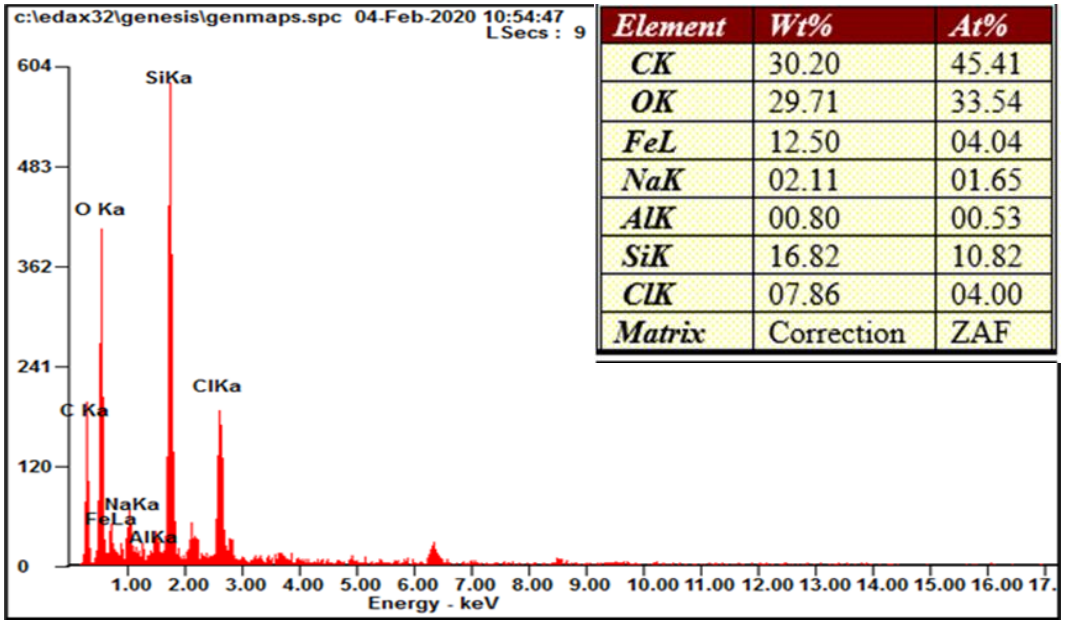

Element	Wt%	At%
CK	30.20	45.41
OK	29.71	33.54
FeL	12.50	04.04
NaK	02.11	01.65
AlK	00.80	00.53
SiK	16.82	10.82
ClK	07.86	04.00
Matrix	Correction	ZAF

Figure 4.9: EDX Analysis of Solid Residue

4.3 Precipitation

There is a total of 2 samples successfully precipitated by combination of 10M, 10ml leaching solution and 0.5M NaOH at different pH values. The initial pH value of 10M leaching solution was 0 and it was increased by adding NaOH into the solution. Reddish-brown precipitate was obtained for pH 5. The precipitate was filtered out and the pH of the remaining solution was increased again by adding NaOH. Subsequently, grey precipitate was obtained at pH 6.34. Table 4.2 shows the samples labelled with 1, 2 and their respective precipitated pH values, weight and volume of NaOH consumed.

Table 4.2: List of Precipitated Samples with Their pH, Weight and Volume of NaOH Consumed

Label	pH	Weight (g)	Volume of NaOH consumed (ml)
1	5.00	0.17	140.7
2	6.34	0.073	4.8
		Total volume of NaOH consumed (ml)	145.5

4.3.1 Physical Appearance and Colour

The physical appearances of the precipitates during the precipitation were illustrated in Figure 4.10.

(a) (b)

Figure 4.10: (a) Reddish Brown Precipitate Settled on the bottom of Slightly Yellowish Solution, (b) Grey Precipitate Suspended in the Slightly Yellowish Solution

All of the prepared samples were then filtered and dried at 80 ℃ for 45 minutes in an oven for further characterization. The colour of dried samples are no longer the same as the colour shown in Figure 4.10 (a), (b). The colour of pH 5 precipitate turned

into dark brown from reddish brown, whereas the colour of pH 6.34 precipitate turned into whitish grey from grey as shown in Figure 4.11 and Figure 4.12.

Figure 4.11: Dried pH 5 Precipitate

Figure 4.12: Dried pH 6.34 Precipitate

Based on the observation, the pH 5 precipitate can be deduced as a solid mixture composed of ferrous hydroxide, $Fe(OH)_3$ and sodium chloride, NaCl. This

explanation is supported by the colour of $Fe(OH)_3$ which ranges from reddish brown to black through dark brown depending on a few factors, for instance particle shape, particle size, crystal structure and the degree of dehydration. It is important to consider that pure NaCl is colourless in nature, however with the presence of $Fe(OH)_3$, its colour would be tainted by the colour of $Fe(OH)_3$. The reaction happened can be shown with the balanced chemical equation below:

$$FeCl_{(3)} + 3NaOH \rightarrow Fe(OH)_3 + NaCl \quad (4.2)$$

Now with the $FeCl_3$ has been precipitated out, it is possible to assume that the remaining solution should only consist of $ZnCl_2$ and other minor elements. Consequently, the pH 6.34 precipitate can be deduced as a solid mixture of zinc hydroxide, $Zn(OH)_2$ and sodium chloride, NaCl. This is because $ZnCl_2$ reacts with NaOH to produce white precipitate of $Zn(OH)_2$.

$$ZnCl_2 + 2NaOH \rightarrow Zn(OH)_2 + 2NaCl \quad (4.3)$$

The whitish grey colour may be resulted by the colour of some impurities, which are the minor elements in the leaching solution.

4.3.2 Characterization of pH 5 Precipitate

The XRD pattern of pH 5 precipitate in Figure 4.13 shows that the pattern can be indexed as sodium chloride (NaCl) and no other phases observed in this precipitate. Sodium chloride peaks are found at 27.68°, 31.97°, 45.70°, 56.79°, 66.62° and 75.44°. The sample has well-defined diffraction patterns with sharp and strong diffraction peaks indicating it is crystalline sample.

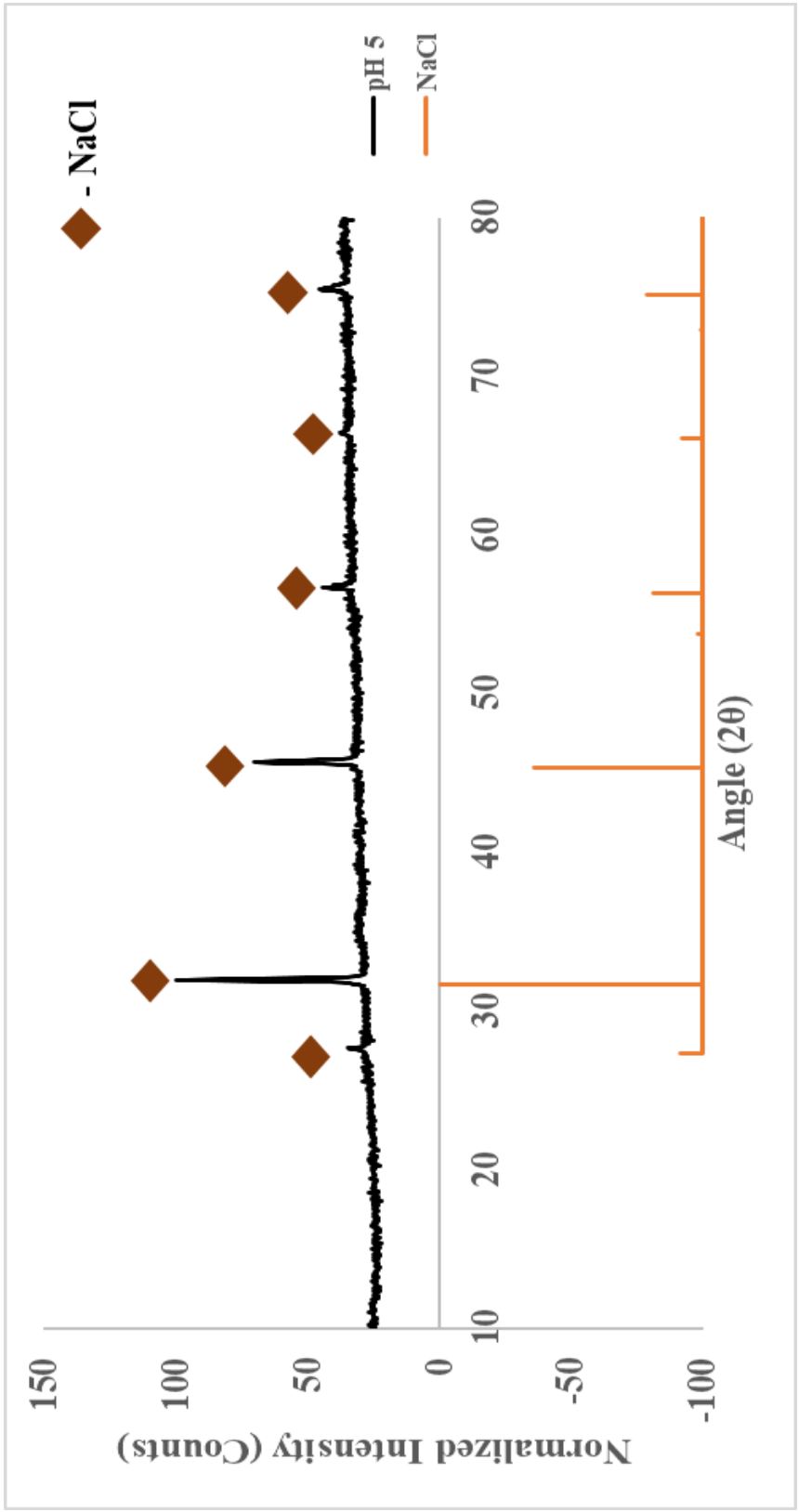

Figure 4.13: XRD Pattern of pH 5 Precipitate

The EDX analysis in Figure 4.14 confirms the presence of sodium chloride in the resulting precipitate. Other than that, small amount of iron is also present in the precipitate. Results of EDX analysis show that the atomic ratio of Na: Cl: Fe in the precipitate obtained has been 19.83%: 16.10%: 1.70%. The results implied that the precipitate is sodium chloride-rich, with iron constituting a minor amount in it. The SEM image (Figure 4.15) indicates that the precipitate consists of agglomerated particles having irregular and smooth surfaces, with a layered morphology.

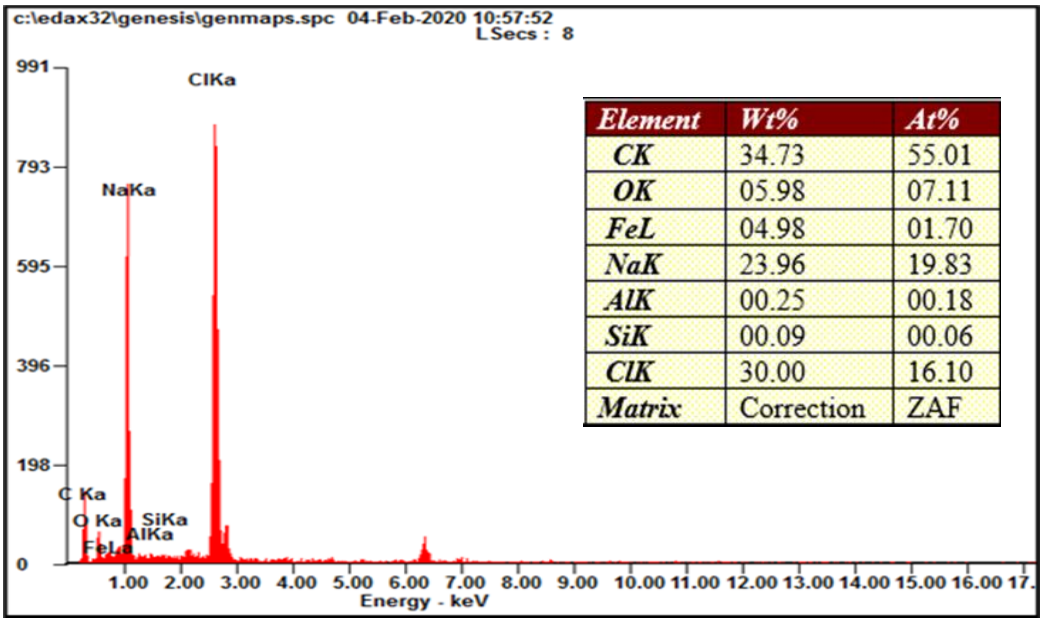

Figure 4.14: EDX Analysis of pH 5 Precipitate

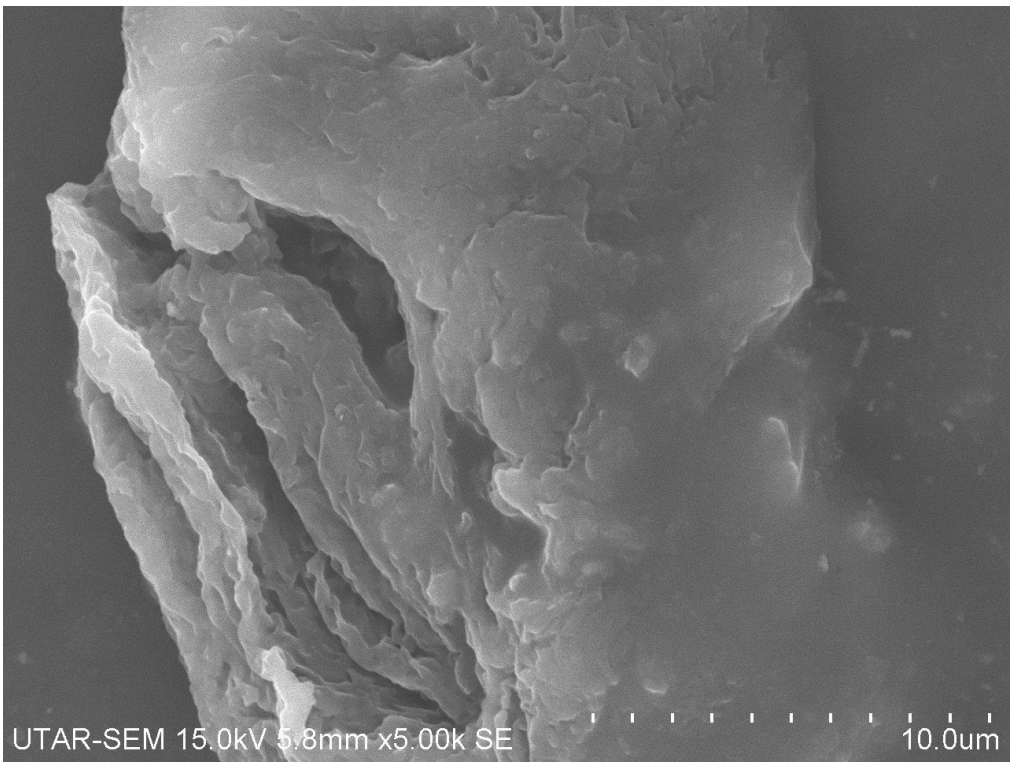

Figure 4.15: SEM Image of pH 5 Precipitate at 5k Magnification

The results from XRD and EDX suggested that iron in the form of oxides or hydroxides was not found in this NaCl-dominant precipitate. The amount of NaCl in precipitate is higher than the amount expected. This result was probably due to the present concentration of leaching solution (10M) and concentration of sodium hydroxide solution (0.5M), the endpoint of precipitation was not reached. Apart from that, it is possible to assume that since most of the NaCl has been precipitated out, pH 6.34 precipitate will be left with less NaCl as impurity. Hence, 21.09 mg of precipitate was sent for TGA analysis in order to uncover the processes that can successfully remove NaCl from the precipitate and form iron oxides at certain temperature.

The thermal decomposition of the sample was determined and analyzed using TGA. The sample were heated from 30 ℃ to 1000 ℃ in nitrogen atmosphere to observe the weight lost due to thermal decomposition. Figure 4.16 shows the TG-DTG curve of pH 5 precipitate**,** while Figure 4.17 shows the DTA curve of pH 5 precipitate.

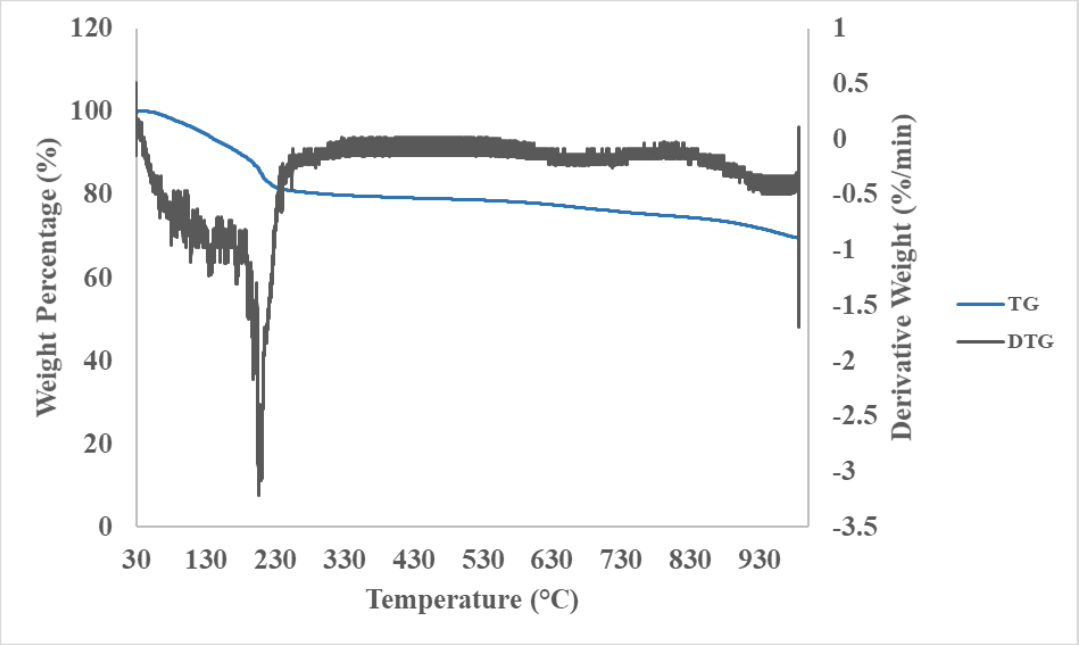

Figure 4.16: TG-DTG Curve of pH 5 Precipitate

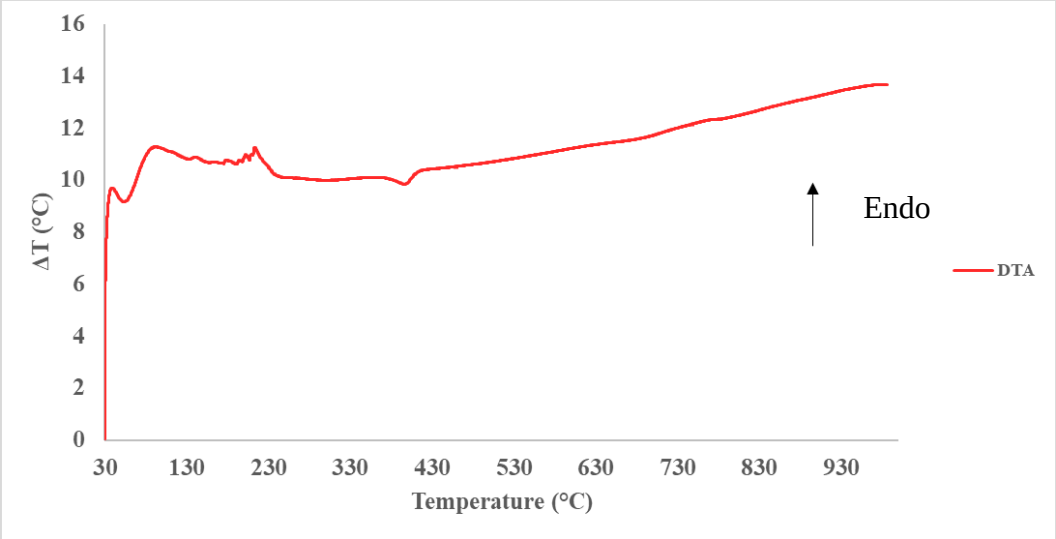

Figure 4.17: DTA Curve of pH 5 Precipitate

Based on the TG curve in Figure 4.16, the first stage of weight loss occurred at the temperature range of 62 ℃ to 290 ℃. The significant weight loss was approximately 20% of the total precipitate weight. No weight loss in precipitate between 290 ℃ to 400 ℃, and 10% weight loss in precipitate at second stage, which was observed at the temperature of 400 ℃ to 1000 ℃. The DTG curve reveals one sharp weight reduction peak corresponding to a decomposition at ~211 °C. On the other hand, the DTA curve demonstrates two endothermic peaks at ~45 °C and ~84 °C

which are interpreted as water losses and one endothermic peak at ~216 °C which is aligned with the sharp weight reduction peak of DTG curve. Besides, one exothermic peak was observed at ~400 $°C$ which will be discussed later. Once the sharp weight reduction temperature was known, the pH 5 precipitate was heated up to 240 ℃ in a tube furnace in a nitrogen atmosphere with heating rate of 7 $℃/min$.

In comparison of characterization results with literatures, the results from work performed by Pinto, Lanza and Lago（2019）on dehydration of ferrous hydroxide, $Fe(OH)_3$ to hematite, Fe_2O_3 which is stated in Literature Review 2.8, is similar with our results in a number of aspects. First and foremost, their TGMS (Thermal Gravimetric Mass Spectrometry) curve with air atmosphere condition in Figure 2.11 shows two endothermic processes: (i) dehydration (water loss) between 100 ℃ and 200 ℃, (ii) dehydroxylation at 234℃.

At 500 ℃, the residue weight for pH 5 precipitate is ~80% as shown in Figure 4.16. The same is also true for the residual weight for $Fe(OH)_3$, which is ~80% at 500 ℃ as shown in the Figure 2.11. The sharp weight reduction peak of pH 5 precipitate at ~216 ℃ correlate fairly with the sharp weight reduction peak of $Fe(OH)_3$ at 234 ℃. From the presented correlation of both results, it may be argued that the pH 5 precipitate analyzed by TGA may contain $Fe(OH)_3$. NaCl is unlikely to be found since NaCl is a crystalline compound held by strong ionic bond which only melts at around 800 ℃.

The XRD analyses for the samples $Fe(OH)_3$ in Figure 2.10 show that for the samples $Fe(OH)_3$ heated above 150 ℃, the presence of hematite, was observed, and as the temperature increased, the hematite peaks became increasingly sharp and narrow, demonstrating an increase in crystallinity. Hence, the exothermic peak of pH 5 precipitate DTA curve at ~400℃ is predicted as recrystallization of a less crystalline hematite to a better crystallized hematite.

Hence, it is crucial to propose that after heating the pH 5 precipitate up to 240 ℃ , with the dehydration and dehydroxylation processes, the pH 5 precipitate will decompose and form hematite Fe_2O_3 eventually. Besides, the SEM images of $Fe(OH)_3$ before heating (Figure 2.12) reported by Pinto, Lanza & Lago (2019) are similar with the SEM image of pH 5 precipitate (Figure 4.15).

4.3.3 Characterization of pH 6.34 Precipitate

The XRD pattern of the pH 6.34 precipitate is shown in Figure 4.18. Peaks at 11.61°, 28.38°, 30.82°, 32.8° and 69.16° are assigned to zinc chloride hydroxide monohydrate, $Zn_5(OH)_8Cl_2 \cdot H_2O$. On the other hand, peaks at 31.74°, 45.60°, 66.63° and 74.94° are assigned to sodium chloride, NaCl. It is apparent that pH 6.34 precipitate consists majorly of $Zn_5(OH)_8Cl_2 \cdot H_2O$ since the three highest intensity peaks are associated with the presence of $Zn_5(OH)_8Cl_2 \cdot H_2O$. This agrees well with the hypothesis that pH 6.34 precipitate has less NaCl compared to pH 5 precipitate.

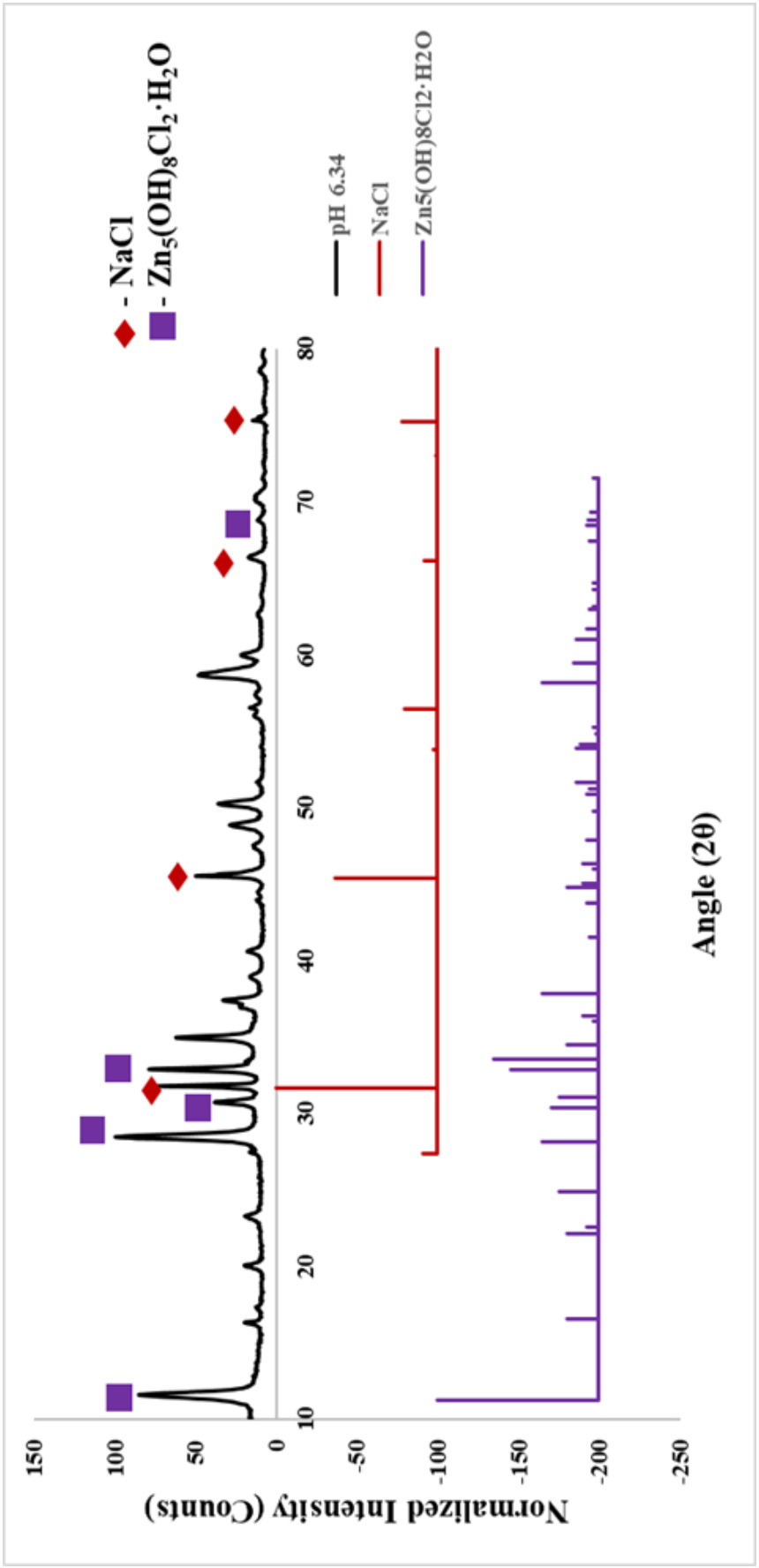

Figure 4.18: XRD Pattern of pH 6.34 Precipitate

TG-DTG and DTA curves of pH 6.34 precipitate are shown in Figure 4.19 and Figure 4.20 respectively when 18.46mg precipitate sample was heated from 30 ℃ to 1000 ℃ in nitrogen atmosphere.

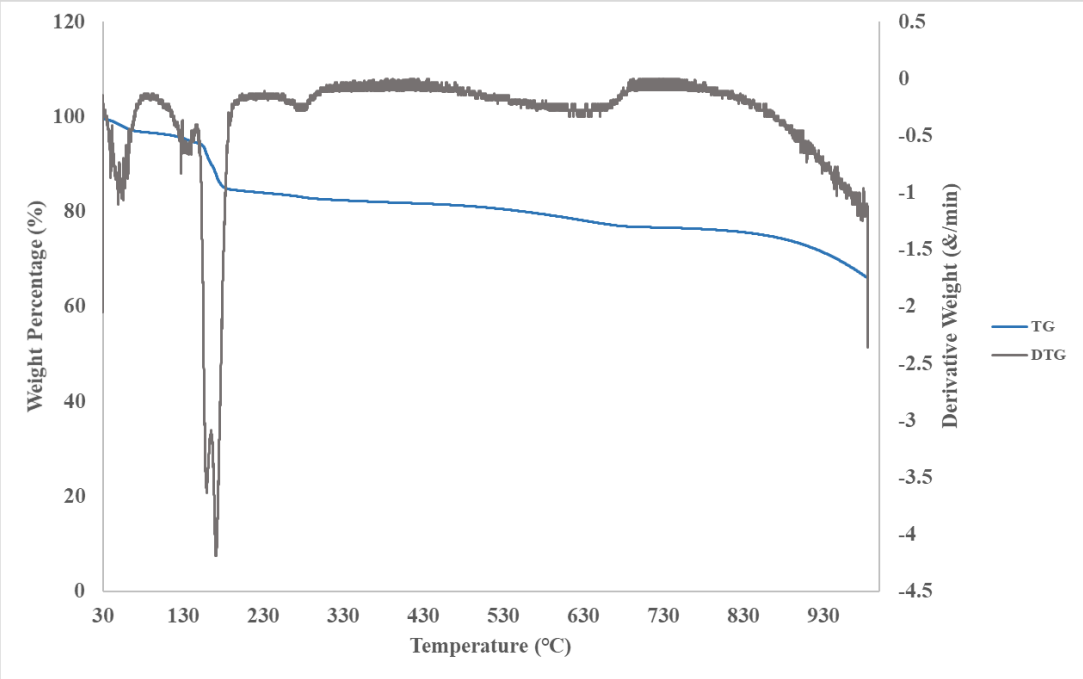

Figure 4.19: TG-DTG curve of pH 6.34 Precipitate

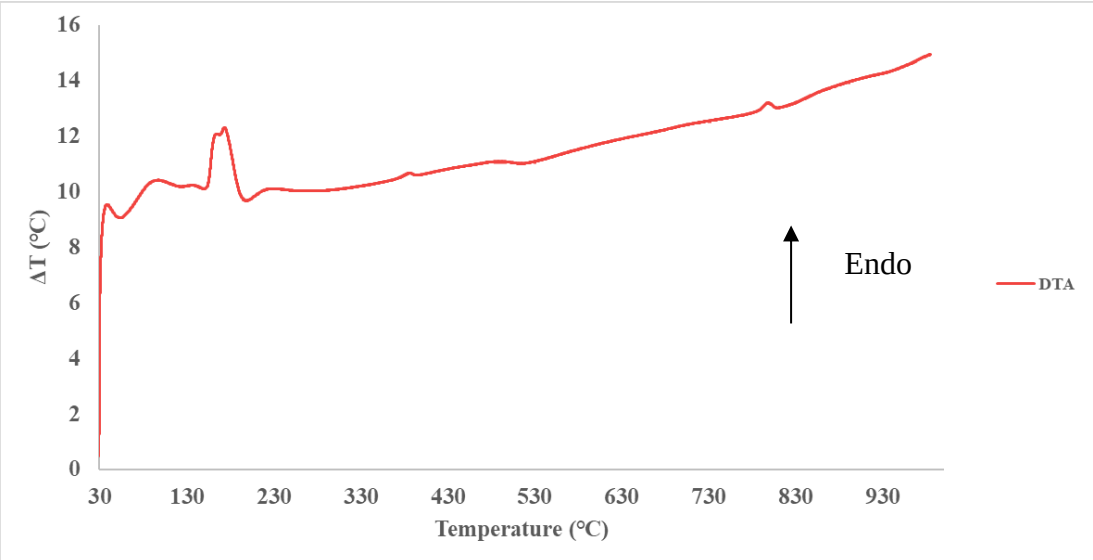

Figure 4.20: DTA curve of pH 6.34 Precipitate

By referring to TG curve in Figure 4.19, there was a significant weight loss for the sample in between 155 ℃ and 186 ℃. At 1000℃, the residual weight is 67% of the

total weight. The DTG curve in Figure 4.19 reveals two sharp weight reduction peaks corresponding to decomposition processes at ~160 °C and ~171 °C. On the other hand, the DTA curve demonstrates six endothermic peaks at ~41 °C, ~103 °C, ~166 °C, ~175 °C, ~395 °C and ~800 °C. Once the sharp weight reduction temperature was known, the pH 6.34 precipitate was heated up to 180 ℃ in a tube furnace in a nitrogen atmosphere with heating rate of 6.3 $℃/min$.

In comparison of characterization results with literatures mentioned in Literature Review 2.9, despite the fact that Rasines and Morales (1979) studied the thermal decomposition in nitrogen atmosphere which is same with our condition, however our endothermic peaks are in good agreement with respect to those reported by Moezzi, Cortie and Mcdonagh (2016). The two endothermic peaks for pH 6.34 precipitate at ~41 °C and ~103° can be attributed to the dehydration of $Zn_5(OH)_8Cl_2 \cdot H_2O$. Moreover, as suggested by Moezzi, Cortie and Mcdonagh (2016), the endothermic peaks at ~166 °C and ~175 °C have been found to be decomposition of $Zn_5(OH)_8Cl_2$ according to Equation 2.12. Apart from that, a small endothermic peak at ~395 °C is validated as thermal decomposition of $Zn(OH)_2.ZnCl_2$ according to Equation 2.14, while the endothermic peak at ~ 800 °C is determined as melting of NaCl.

It has proven that by heating the pH 6.34 precipitate to 180 ℃, ZnO can be successfully formed and the chloride composition can be separated. On the basic of comparison of results with literature data, it is noteworthy that there will be difference in temperature range for thermal behavior of $Zn_5(OH)_8Cl_2 \cdot H_2O$ in the precipitate as the $Zn_5(OH)_8Cl_2 \cdot H_2O$ used by Moezzi, Cortie and Mcdonagh (2016) do not contain any other impurities.

4.4 Summary

In summary, there are two main experiments in the study. In leaching experiment, using HCl as leaching agent, the experiment was done at 10M, 50 ℃. The characterization results of resultant leaching solution suggest that the maximum extraction percentages of Zn and Fe were obtained with > 90%. The results of EAFD and solid residue from XRD and EDX were compared, the methodology has been proven to be successful in extracting Zn and Fe, leaving carbon as the solid residue.

SEM results show spherical-shaped particles of EAFD become irregular-shaped after leaching.

Two precipitates have been formed from 10M, 10 ml leaching solution using 0.5M NaOH as precipitating agent. The precipitates were formed at pH 5 and pH 6.34 respectively. Dried pH 5 precipitate was dark brown in colour, while dried pH 6.34 precipitate was whitish grey in colour. Initially, pH 5 precipitate was hypothesized to be made up of $Fe(OH)_3$ and NaCl, nonetheless the results from XRD and EDX validate the precipitate is NaCl-rich, with only 1.7 at% of Fe as analyzed by EDX. A closer comparison of TGA results with literature revealed that the precipitate may contain $Fe(OH)_3$ because the endothermic peaks are related to dehydration and dehyroxylation of $Fe(OH)_3$. One exothermic peak is suggested for recrystallization of hematite. Moreover, there is no peak showing the melting and boiling of NaCl.

XRD results demonstrate pH 6.34 precipitate was comprised of $Zn_5(OH)_8Cl_2{\cdot}H_2O$ and NaCl. Through comparing TGA results with literature, the endothermic peaks of the precipitate are related to thermal transformation of $Zn_5(OH)_8Cl_2{\cdot}H_2O$ in precipitation to ZnO.

CHAPTER 5

CONCLUSIONS AND RECOMMENDATIONS

5.1 Conclusion

The mineralogical and chemical composition of EAFD were identified to be composed mainly of Zn and Fe compounds in the following phases: $ZnFe_2O_4$, Fe_3O_4 and ZnO. Zn and Fe extraction from EAFD using HCl was investigated successfully in this project. Maximum Zn and Fe extraction percentage, 94.36% and 95%, were achieved at the following conditions: 10 M HCl, 50 °C leaching temperature, 15 minutes leaching duration, 700 rpm stirring speed, and dust-to-acid ratio of 1:30. Reddish-brown colour of leaching solution was caused by the rich presence of $FeCl_3$. The leaching solution contained 69.26 mg/L of Zn and 132.3 mg/L of Fe which can be precipitated out by NaOH afterwards. Nevertheless, the result of HCl fume recycling was unfavorable as the leaching temperature in this project was limited to 50 ℃, which was inadequate to vaporize HCl solution completely.

By 0.5M NaOH precipitation via increasing the pH of leaching solution from 0 to 14 with 400 rpm stirring speed in room condition, NaCl and $Fe(OH)_3$ were precipitated at pH 5, while $Zn_5(OH)_8Cl_2 \cdot H_2O$ and NaCl were precipitated at pH 6.34. XRD and EDX results can confirm that the pH 5 precipitate is essentially composed of NaCl. This result can be justified by the endpoint of the precipitation was not reached. It is difficult to arrive at any conclusions with regard to whether the dark brown colour of pH 5 precipitate was resulted from $Fe(OH)_3$. However, with the examination and comparison with literature data on TG-DTG and DTA curves, the results have been broadly translated to indicate that there was presence of $Fe(OH)_3$ in minority for several reasons: (i) the endothermic peaks at ~45 °C and ~84 °C are interpreted as dehydration of $Fe(OH)_3$, (ii) the endothermic peak at ~216 °C is attributed to dehydroxylation processes of $Fe(OH)_3$ to form Fe_2O_3, (iii) the exothermic peak at ~400 ℃ is predicted as recrystallization of hematite with lower crystallinity to a hematite with higher crystallinity, (iv) NaCl has strong ionic lattice which can only be thermally decomposed at its melting point (801 °C) and boiling point (1,465 °C).

For pH 6.34 precipitate, the XRD results disclosed that $Zn_5(OH)_8Cl_2 \cdot H_2O$ was found notably in the precipitate with its three highest peaks, while minor amount of NaCl was also present in the precipitate, which meet the expectation, since most of the NaCl has been precipitated out at pH 5. The endothermic peaks of DTA curve match well with literature, in which the peaks at ~41 °C and ~103 °C highlight the dehydration of $Zn_5(OH)_8Cl_2 \cdot H_2O$, the peaks at ~166 °C and ~175 °C underline the decomposition of $Zn_5(OH)_8Cl_2$ and the peak at ~395 °C demonstrates decomposition of $Zn(OH)_2.ZnCl_2$. In general, thermal transformation of $Zn_5(OH)_8Cl_2 \cdot H_2O$ in precipitation to ZnO went through the formation of $Zn_5(OH)_8Cl_2$, $ZnO.ZnCl_2.2H_2O$ and $Zn(OH)_2ZnCl_2$ as intermediate products. It is also fundamental to note that one endothermic peak at ~ 800 °C is suggested as melting of NaCl.

Each precipitate was heated to their determined sharp weight reduction temperatures respectively in a tube furnace in nitrogen atmosphere. The results of this project have highlighted the devised methodology clearly has an advantage over to form Fe_2O_3 and ZnO as well as to separate the chlorides in the end. The present results might have important implications for solving EAFD waste problem in steelmaking industry.

5.2 Recommendations for Future Work

Throughout this research project, there are some recommendations that can be considered to improve future work.

i. Pressure leaching of EAFD with HCl can be performed to increase the efficiency of leaching.
ii. Employing deionized water as the main washing solvent to remove NaCl on the surface of the precipitate as it can effectively dissolve the NaCl at room temperature.
iii. Employing larger amount of leaching solution for precipitation in order to increase the weight of yield produced.
iv. Performing XRD and SEM-EDX of the precipitates after heating to compare the chemical composition and microstructures before and after heating.
v. To study the precipitation performance using other alkali solvents such as sodium bicarbonate, $NaHCO_3$.

vi. Employing different concentration of NaOH solution so the endpoint of precipitation can be reached.

REFERENCES

Al-Makhadmeh, L.A., Batiha, M.A., Al-Harahsheh, M.S., Altarawneh, I.S. & Rawadieh, S.E. 2018, 'The Effectiveness of Zn Leaching from EAFD Using Caustic Soda', *Water, Air, and Soil Pollution*, vol. 229, no. 2.

Aula, M., Haapakangas,J., Heikkilä,A., and Iljana.M., 2012, *Some environmental aspects of BF , EAF and BOF*. Available at: < https://www.researchgate.net/publication/236670733_Some_environmental_aspects_of_BF_EAF_and_BOF >

Bunaciu, A.A., Udriştioiu, E. gabriela & Aboul-Enein, H.Y. 2015, 'X-Ray Diffraction: Instrumentation and Applications', *Critical Reviews in Analytical Chemistry*, vol. 45, no. 4, pp. 289–99.

Chong, C.S., 2019, *Extraction of Zinc and Iron from Electric Arc Furnace (EAF) Dust Waste.* Final Year Project, UTAR.

EU-MERCI. 2020, *Technical analysis – Iron and Steel*, no. 693845.

Farag, R.K. 2015, 'Hydrogel Nanoparticles: Synthesis and Characterization', *Encyclopedia of Biomedical Polymers and Polymeric Biomaterials*, vol. 5, pp. 3808–16.

Guwahati, I., 2014. *Catalysts Preparation-Precipitation*. [online] Available at: <https://nptel.ac.in/courses/103/103/103103026/> [Accessed 3 July 2019].

Gorodylova, N., Cousy, S., Šulcová, P. and Svoboda,L. *Thermal transformation of layered zinc hydroxide chloride*. *J Therm Anal Calorim* 127, 675–683 (2017).

Hagen, J.P. & Sneddon, J. 2009, 'Determination of copper, iron, and zinc in crayfish (Procambrus clarkii) by inductively coupled plasma-optical emission spectrometry', *Spectroscopy Letters*, vol. 42, no. 1, pp. 58–61.

Havlik, T., Turzakova, M., Stopic, S. & Friedrich, B. 2005, 'Atmospheric leaching of EAF dust with diluted sulphuric acid', *Hydrometallurgy*, vol. 77, no. 1–2, pp. 41–50.

Irfan, S., Ajaz-Un-Nabi, M., Jamil, Y. & Amin, N. 2014, 'Synthesis of Mn1-xZnxFe2O4 ferrite powder by co-precipitation method', *IOP Conference Series: Materials Science and Engineering*, vol. 60. https://doi.org/10.1088/1757-899X/60/1/012048

Julieth, L., Buitrago, H., Prada, I.D. & Amaral-labat, G. 2018, *Microstructural , thermochemistry and mechanical evaluation of self-reducing pellets using electric arc furnace (EAF) dust containing zinc for Waelz process*, Matéria (Rio

J.), 2018, vol.23, n.2, e-12006. https://doi.org/10.1590/s1517-707620180002.0343.

Kennison, S. 2014, *How Steel is Made Using the Basic Oxygen Steelmaking Process*. Available at :< http://seankennison.weebly.com/uploads/2/8/6/7/28671267/basic_steelmaking_process.pdf>

Lee, H.S., Park, D.S.M., Hwang, Y., Ha, J.G. & Shin, H.S. 2019, 'Toward high recovery and selective leaching of zinc from electric arc furnace dust with different physicochemical properties', *Environmental Engineering Research*, pp. 0–2.

Lin, X., Peng, Z., Yan, J., Li, Z. & Hwang, J. 2017, 'Pyrometallurgical recycling of electric arc furnace dust', *Journal of Cleaner Production*, vol. 149, pp. 1079–100.

Martín, A.N., 2015, *Development of hydrometallurgical processes for zinc recovery from steelmaking waste*. Available at: <https://addi.ehu.es/bitstream/handle/10810/21046/TESIS_ANTU%c3%91ANO_MARTIN_NESTOR.pdf?sequence=4&isAllowed=y>

Marwaha, N., Gupta, B.K., Verma, R. & Srivastava, A.K. 2017, 'Facile synthesis and characterization of pH-dependent pristine MgO nanostructures for visible light emission', *Journal of Materials Science*, vol. 52, no. 17, pp. 10480–4.

Moezzi, A., Cortie, M. and Mcdonagh, A. 2016, *Transformation of Zinc Hydroxide Chloride Monohydrate to Crystalline Zinc Oxide, Dalton Trans., 2016,45, 7385-7390*

Mohanraj, K. and Sivakumar, G. 2017, 'Synthesis of γ-Fe2O3, Fe3O4and Copper Doped Fe3O4nanoparticles by sonochemical method', *Sains Malaysiana*, vol. 46, no. 10, pp. 1935–42.

Nanakoudis, A., 2019. *EDX Analysis with a Scanning Electron Microscope (SEM): How Does it Work?* [online] Available at: <https://blog.phenom-world.com/edx-analysis-sem>

Palimąka, P., Pietrzyk, S., Stępień, M., Ciećko, K. & Nejman, I. 2018, 'Zinc Recovery from Steelmaking Dust by Hydrometallurgical Methods', *Metals*, vol. 8, no. 7, p. 547.

Pinto, P.S., Lanza, G.D. and Lago, R.M. 2019, *Controlled Dehydration of Fe(OH) 3 to Fe $_2$ O $_3$: Developing Mesopores with Complexing Iron Species for the Adsorption of β -Lactam Antibiotics, Journal of the Brazilian Chemical Society*, vol. 30, No. 2, pp. 310-317.

PubChem, n.d., *Ferric chloride*. [online] Available at:< https://pubchem.ncbi.nlm.nih.gov/compound/Ferric-chloride>

Rasines,I. and Morales,J.L., 1979. *Thermal Analysis of* β -$CO_2(OH)_3Cl$ *and* $Zn_5(OH)_8Cl_2{\cdot}H_2O$. *Thermochimica Acta 1980*, vol. 37; Iss. 2,pp.239-246

Schaffer,J. and Herman,C., 2019. *Precipitation and the Solubility Product*. [online] Available at:<https://chem.libretexts.org/Bookshelves/General_Chemistry/Map%3A_Principles_of_Modern_Chemistry_(Oxtoby_et_al.)/UNIT_4%3A_EQUILIBRIUM_IN_CHEMICAL_REACTIONS/16%3A_Solubility_and_Precipitation_Equilibria/16.3%3A_Precipitation_and_the_Solubility_Product> [Accessed 1 August 2019].

Shawabkeh, R.A. 2010, 'Hydrometallurgical extraction of zinc from Jordanian electric arc furnace dust', *Hydrometallurgy*, vol. 104, no. 1, pp. 61–5.

Simonyan, L.M., Alpatova, A.A. & Demidova, N. V. 2019, 'The EAF dust chemical and phase composition research techniques', *Journal of Materials Research and Technology*, vol. 8, no. 2, pp. 1601–7.

Sofilić, T., Rastovčan-Mioč, A., Cerjan-Stefanović, Š., Novosel-Radović, V. & Jenko, M. 2004, 'Characterization of steel mill electric-arc furnace dust', *Journal of Hazardous Materials*, vol. 109, no. 1–3, pp. 59–70.

Tauriainen, M. 2015, *Decomposition of zinc ferrite from waste streams of steelmaking*. Available at :< http://jultika.oulu.fi/files/nbnfioulu-201512022191.pdf >

Teo, Y.Y., Lee, H.S., Low, Y.C., Choong, S.W. & Low, K.O. 2017, 'International Conference on Environmental Research and Technology (ICERT 2017) *International Conference on Environmental Research and Technology*, vol. 1, no. Icert, pp. 281-286.

Teo, Y.Y., Lee, H.S., Low, Y.C., Choong, S.W. & Low, K.O. 2018, 'Hydrometallurgical extraction of zinc and iron from electric arc furnace dust (EAFD) using hydrochloric acid', *Journal of Physical Science*, vol. 29, pp. 49–54.

Trunschke, A., 2011, *Synthesis of Catalysts: A brief overview* * , [online] Available at : <http://www.fhi-berlin.mpg.de/acnew/department/pages/teaching/pages/teaching__wintersemester__2011_2012/annette_trunschke__catalyst_synthesis__111118.pdf >

Wang, Z., Li, H., Tang, F., Ma, J. & Zhou, X. 2018, 'A Facile Approach for the Preparation of Nano-size Zinc Oxide in Water/Glycerol with Extremely Concentrated Zinc Sources', *Nanoscale Research Letters*, vol. 13, pp. 1–9.

York, O.N., Auckland, A., Bogod, B., Aires, B., Town, C., Dares, C., Delhi, S., Hong, F., Istanbul, K., Kuala, K., Madrid, L., Mumbai, C., Paris, N., Paulo, S. & Toronto, T. 1999, *the Making of iron and steel*, vol. 0, pp. 1–50.

APPENDICES

APPENDIX A: Graphs

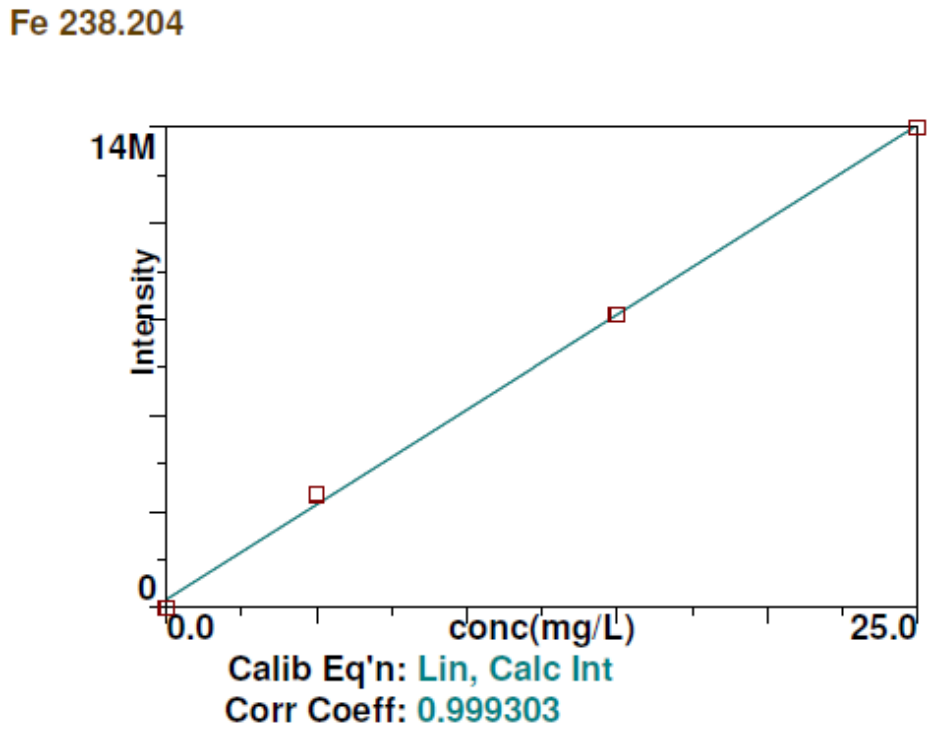

Graph A-1: Calibration Curve of Iron Standard Solution in ICP-OES with Correlation Coefficient of 0.999303.

APPENDIX B: Pictures

Calibration Summary

Analyte	Stds.	Equation	Intercept	Slope	Curvature	Corr. Coef.
Zn 206.200	3	Lin, Calc Int	17880.9	61490	0.00000	0.999353

Picture B-1: Calibration Summary of Zinc in Standard Solution in ICP-OES with Correlation Coefficient of 0.999353.

Picture B-2: Fisher Scientific 37% HCl solution

Picture B-3: Fisher Scientific NaOH Pellets

Picture B-4: ESCO Drying Oven

Picture B-5: Perkin Elmer Optima 7000 Inductively Coupled Plasma-Optical Emission Spectrometer (ICP-OES)

Picture B-6: Shimadzu XRD-6000 X-Ray Diffractometer (XRD)

Picture B-7: Hitachi S-3400N Scanning Electron Microscope (SEM)